The Deflection and Division of an Oceanic Baroclinic Jet by a Coastal Boundary: A Case Study in the Alboran Sea

ÁLVARO VIÚDEZ* AND ROBERT L. HANEY

Department of Meteorology, Naval Postgraduate School, Monterey, California

JORGE VÁZQUEZ-CUERVO

Jet Propulsion Laboratory, Pasadena, California

(Manuscript received 20 June 1996, in final form 5 June 1997)

ABSTRACT

An oceanic baroclinic jet impinging on a coastal boundary represents a particular type of ocean–coast interaction. This specific oceanographic phenomenon is an example of the stagnation in line flows occurring in fluid dynamics with three additional features: rotation, stratification, and a sloping boundary. In this study the authors describe the density, vorticity, and deformation characteristics of an oceanic jet impinging on a sloping boundary. The case study corresponds to the impinging process of the Atlantic jet at the African coast (Alboran Sea).

In the impinging region, the acceleration field is divergent related to the fact that the magnitude of the deformation is larger than the magnitude of the rotation. It is also found that the stagnation streamsurface does not lie in a vertical plane but tilts in the opposite direction to the tilt of the isopycnals. The flow upstream of the stagnation point is characterized by backing, speed convergence, diffluence, and negative streamwise vorticity. The flow past the stagnation point is characterized by veering, speed divergence, confluence, and positive streamwise vorticity. The current can only be considered irrotational in a narrow part of the impinging region.

1. Introduction

The nature of the oceans, as masses of fluid interacting with solid boundaries, makes possible, as a particular type of ocean–coast interaction, the phenomenon of an oceanic jet impinging on a coastal boundary. Among the many consequences produced by such an interaction, two features are of principal importance for the jet and its surroundings. These are its evident deflection by the coastal boundary and its division into two branches flowing along the coast. In the steady state, which is the case considered in this work, the phenomenon is observed only in specific oceanic regions having suitable boundary conditions, for instance at the exits of straits where a permanent outflow approaches the continental shelf. This specific oceanographic phenomenon is an example of the stagnation in line flows studied in fluid mechanics. A brief summary of these flows will help to define the objective of this work and to place it in perspective with other branches of that discipline.

Following the classic boundary-layer theory for the solution of the two-dimensional incompressible steady flow of a homogeneous fluid near a stagnation point at a rigid boundary, it is convenient to divide the flow into the potential (irrotational) and the viscous (with nonzero vorticity) regions (Fig. 1). The flow $\mathbf{v}_\psi$ in the irrotational region is known to be described by the streamfunction $\psi = kxy$, where k is a positive constant and $\mathbf{v}_\psi = -\mathbf{k} \times \text{grad}_h \psi$ [see also other possible streamfunctions in, e.g., Peregrine (1981), Dorrepaal (1986), and Pedlosky (1987, p. 94)]. For the viscous region the governing Navier–Stokes equations can be reduced to an ordinary differential equation leading to similarity solutions. That solution was obtained numerically by Hiemenz (1911) and improved upon by Howarth (1935) [see, e.g., Batchelor (1970, chap. 5.5); Schlichting (1979) chap. V); Churchill (1988, chap. 14)]. Since that time, two-dimensional steady flow with a stagnation point has been referred to as ''Hiemenz flow.'' A similar division may be adopted in the oceanographic context. An oceanic jet approaching a continental slope has smaller turbulent eddy coefficients in the open ocean region than in the coastal region over the continental shelf. We will be primarily concerned with the changes experienced by such an oceanic free jet as it approaches the coast seaward of the 200-m isobath. Two important assumptions

* Current affiliation: Departament de Física, Universitat de les Illes Balears, Palma de Mallorca, Spain.

Corresponding author address: Álvaro Viúdez, Departament de Física, Universitat de les Illes Balears, 07071—Palma de Mallorca, Spain.
E-mail: DFSAVL4@PS.UIB.ES

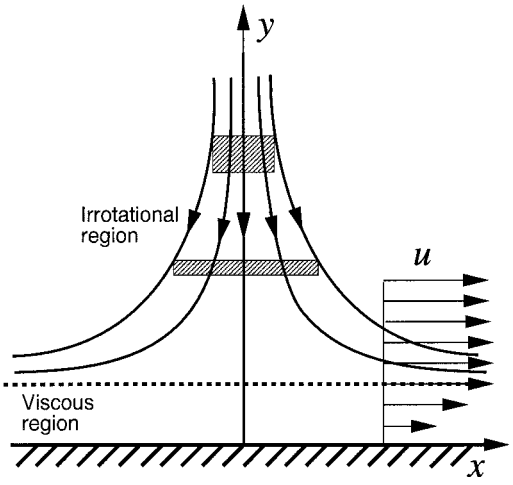

FIG. 1. Schematic showing the irrotational and viscous regions of the two-dimensional incompressible steady flow of a homogenous fluid near a stagnation point. The dashed area represents a fluid element.

can therefore be justified for this situation. The first is that, as mentioned above, the flow is considered inviscid. The second is that the bottom depth is everywhere large enough to allow geostrophic velocities referred to a horizontal layer (e.g., at 200 m) of nearly zero motion to be computed from the density field. Unlike the theoretical jet studied by Hiemenz, oceanic jets cannot in general be considered irrotational. On the one hand, oceanic jets have large vertical shear and therefore a large horizontal component of relative vorticity. On the other hand, the vertical component of the relative vorticity even in straight impinging jets (i.e., ones with zero curvature vorticity) may be large due to the horizontal shear (shear vorticity).

The interest in quasi two-dimensional impinging flows having vorticity lies in the fact that the vorticity component parallel to the streamlines is susceptible to amplification by stretching and thus may be intensified near the boundary. The first studies of impinging two-dimensional flows with vorticity in the inviscid region were made in the context of the aeronautical sciences (Ferri and Libby 1954). Stuart (1959), after the studies of Li (1955, 1956) and Glauert (1957), considered the influence of uniform vorticity perpendicular to the plane of the two-dimensional flow of the fluid in the viscous region (such a fluid flow undergoes no stretching). Rott and Lenard (1959) and Kemp (1959) studied the same phenomenon but for axisymmetric stagnation flows. The effects of vorticity having a particular orientation susceptible to amplification by stretching when transported into the stagnation point boundary (turbulent) layer were described using a mathematical model by Sutera et al. (1963) and Sutera (1965). They demonstrated the possibility of vorticity amplification by stretching in quasi two-dimensional stagnation flow when the vorticity scale is larger than a certain neutral scale.

With the help of the above comments concerning general stagnation jets we are in a position to define this work as the study of the changes that a free jet with vorticity experiences when it approaches a solid boundary. Therefore, this work deals with the so-called *external flow*, that is, outside the viscous (turbulent) stagnation region, but such an external flow having vorticity. Furthermore, the geophysical context provides three new features that have not been addressed previously: namely, rotation, stratification, and a sloping boundary. To our knowledge the first work to address some consequences of the stagnation point region of a water jet in rotating fluid mechanics was that by Whitehead and Miller (1979) and later by Whitehead (1985a) in a laboratory simulation of the western Alboran gyre (WAG) in the Alboran Sea (Western Mediterranean) and the uplift near the Strait of Gibraltar. They pointed out that the growth of the gyre in their simulations may be due to the position of the stagnation point of the jet relative to coastal features at the point where the jet impinges on the African coast. They were unable to identify the existence of any theoretical or experimental studies of the properties of stagnation point flows in baroclinic, rotationally influenced jets. Whitehead considered the deflection by a vertical wall of a jet in a rotating fluid of constant density lying over a motionless fluid of slightly higher density. Using a momentum integral and considering a zero- as well as a constant-potential-vorticity jet, Whitehead was able to determine the relative size of the two branches of split flow as a function of the angle of incidence of the external jet.

The aim of this work is to characterize from observations the density and velocity changes experienced by a free, nearly geostrophic jet when it impinges on a sloping coastal boundary. We will therefore focus, as mentioned above, on the oceanic jet seaward of the continental shelf. We are aware that this topic is too wide and too complex to be resolved in one study. Consequently, our attempt is to describe the main hydrographic and kinematic properties that we have found to be clearly present in the impinging process. Therefore, the dynamical properties are excluded in this work. The specific case chosen in this study is the same one that motivated Whitehead's studies, that is, the stagnation in line flow of the Atlantic current in the Alboran Sea. The description of the observations (section 2) is based on the density as well as on the vorticity and deformation fields. Due to the presence of a sloping coastal boundary, the changes in the jet's structure occur in both the horizontal and vertical directions, that is, the changes are of a three-dimensional nature. Section 3 is devoted to the discussion and conclusions, and section 4 to the summary.

2. A case study: The Atlantic current in the Alboran Sea

The Atlantic current impinging on the African coast in the Alboran Sea is probably one of the best examples

in nature of a quasi-steady jet impinging on a coast. Another possible example is the flow exiting the Tsugaru Strait north of Japan (Conlon 1982; Kawasaki and Sugimoto 1984). In both cases the geographic permanence of a jet is assured by a strait's outflow. The knowledge of the physical oceanography of the Alboran Sea, although by no means complete, is one of the most extensive in the entire Mediterranean. The reader is referred to Parrilla and Kinder (1987) for a general description, Bucca and Kinder (1984) for meteorological effects, Gascard and Richez (1985) and Parrilla et al. (1986) for water masses, La Violette (1986) for short-term variability, Heburn and La Violette (1990) for gyre's variability, Perkins et al. (1990) for the Atlantic inflow, Viúdez et al. (1996a, 1996b) for the gyre's structure and ageostrophic motion, and Vázquez-Cuervo et al. (1996) for altimeter data analysis (and references therein).

The present data consists of 134 CTD stations ($\Delta x \approx 30$ km, $\Delta y \approx 18$ km) acquired in the Alboran Sea in September 1992 [described in detail in Viúdez et al. (1996a)]. Partial use is made of altimeter data [*ERS1* (European Remote Sensing satellite) and TOPEX/Poseidon (ocean TOPography EXperiment)] in the discussion section in order to address the long-term temporal variability of the impinging process.

It has been the custom for ease of reference (e.g., La Violette 1986; Viúdez et al. 1996a) to use the term Atlantic jet (AJ) for the flow that, entering through the Strait of Gibraltar, usually impinges on the African coast at 3°40′W (Fig. 2). This flow then deflects to the left (facing downstream) and enters the eastern Alboran basin and then into the Algerian basin. The term WAG refers to the closed circulation including the flow that is deflected to the right at the stagnation point at the African coast. Strictly, the AJ and WAG are not two independent physical systems since there is water interchange between them (Lanoix 1974; Viúdez et al. 1996a). Since, in fact, they share a common density front, the current associated with this density front is here referred to as the impinging current, impinging jet, or simply the current, in order to distinguish it from the AJ (the impinging current being wider than the AJ). Using this terminology, the current impinges on the sloping African coast and is deflected and divided into two branches: the AJ, or left branch, and the WAG current, or right branch. Note that the horizontal and vertical scales of the African continental shelf in the impinging region (~15 km and 200 m, respectively; see, e.g., Fig. 3) are of the same order as the horizontal and vertical scales of the Atlantic jet (or the impinging current). Thus, we expect that the sloping of the shelf influences the impingment process. Furthermore, since the width of the shelf is comparable to the meridional distance between CTD stations (~18 km), we expect also that this influence may be detectable in the hydrographic data. Other possible features associated with the impinging process, but having spatial scales smaller than the spacing between CTD stations, could be missed or aliased with the present data resolution.

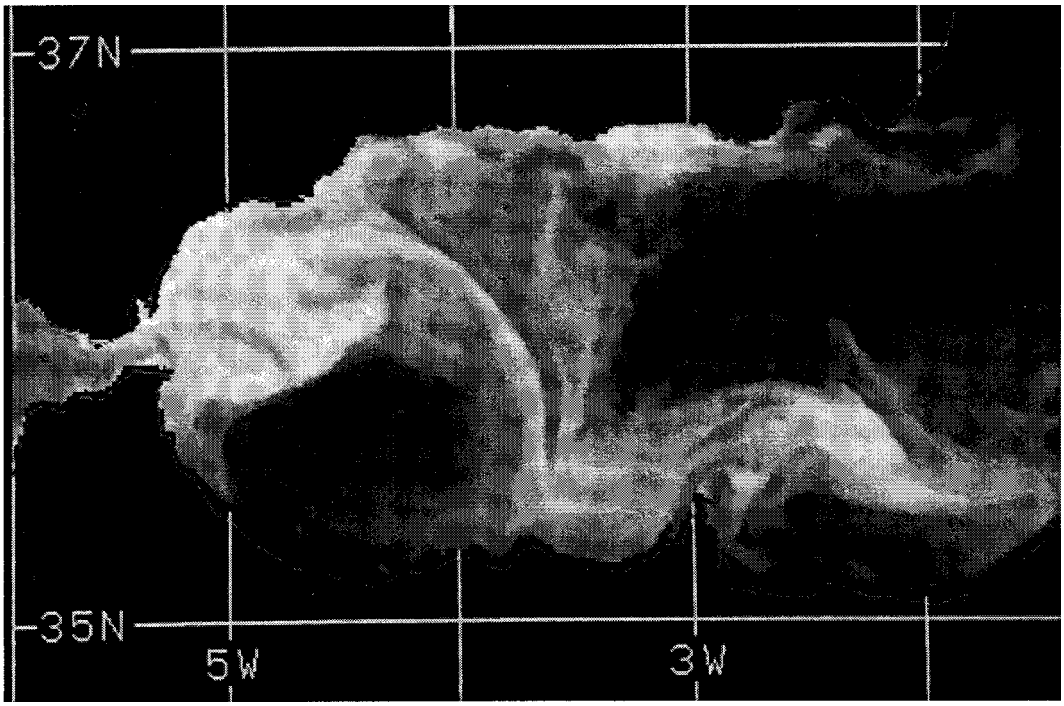

FIG. 2. A typical satellite thermal image of the impinging current in the Alboran Sea. Light grayscale means relatively cold water.

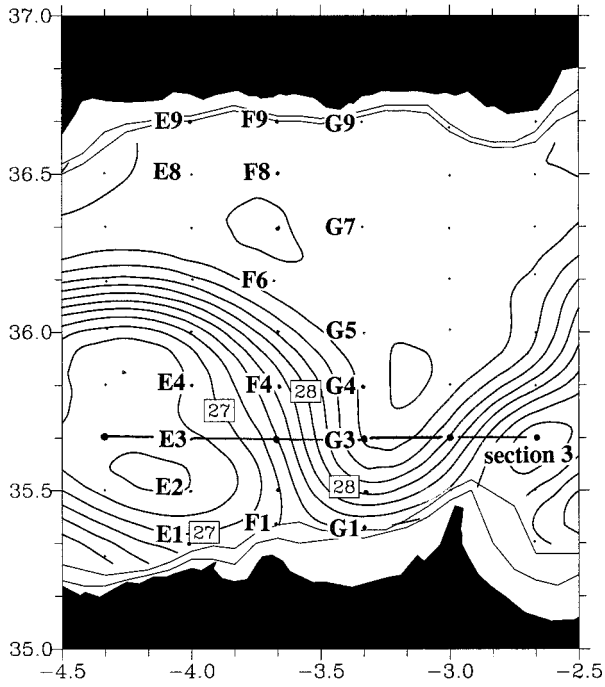

FIG. 3. Potential density (σ_θ) distribution at 100 m. The dots indicate CTD stations. Several vertical sections are also referenced. The coastal bathymetry (100 m and 200 m) is also indicated. Labels on the horizontal and vertical axes indicate longitude and latitude, respectively, in degrees.

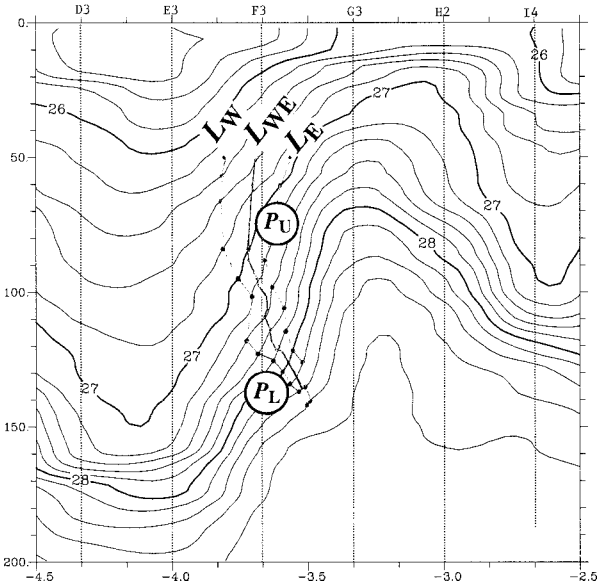

FIG. 4. Potential density (σ_θ) distribution at vertical section 3 (see Fig. 3). The right (L_E) and left line (L_W) join the σ_θ values found at the same depth in the two CTD stations closest to the coast after the flow division (stations E1 and G1 in Fig. 3). The central line (L_{WE}) identifies the approximate stagnation streamsurface. Labels on the vertical axis indicate the depth in meters.

a. Hydrography

The hydrographic data can give us information about the splitting of the impinging current on the African coast (Fig. 3). Consider the σ_θ distribution on a cross-front vertical section of the current before its division into two branches (Fig. 4). Superimposed on this distribution we have indicated with dots the σ_θ values, between 50 and 150 m, found at the two CTD stations closest to the coast after the flow division (station E1 and G1 in Fig. 3). If, for this distance between CTD stations (~30 km) at this depth (~100 m), vertical displacement and diabatic terms in the conservation of potential density are neglected, the curves L_W and L_E linking these dots separate water that is to be deflected eastward (line L_E) from the water to be deflected westward (line L_W). The deflection of the fluid between line L_W and L_E cannot be determined from the CTD data. This amount of *missing* water, which produces the uncertainty in the determination of the direction of deflection, flows between the coast and the closest CTD stations offshore; that is, this flow cannot be resolved for the given location of the CTD stations. Note that due to the slope of the coast, this uncertainty decreases with depth. Line L_{WE}, defined as equidistant to L_W and L_E in the horizontal, is therefore an approximation to the intersection of the stagnation streamsurface of the impinging current with the plane of vertical section 3. This line L_{WE} represents, therefore, the division of the impinging current into the AJ and the WAG. Two important results can be drawn from this flow division. The first one is that the AJ flows eastward associated with a density front that is basically confined to the first 150 m (Fig. 5c), while the WAG water flows westward with the largest density gradients below 100 m (Fig. 5a). Note also the reversed baroclinicity [the slopes of isopycnals change sign with depth (Onken 1990)] in vertical section F (Fig. 5b) in between stations F4 and F2. The consequences that this reversed baroclinicity have in the vertical shear will be described in the next section.

The second result is that L_{WE} has some tilt. This shows that the stagnation streamsurface does not lie in a vertical plane but tilts in the direction defined by the density gradients, the tilting tending to be diapycnal rather than isopycnal, that is, opposite to the vertical tilting of isopycnals. This tilting of the stagnation streamsurface is assured, in spite of the rather coarse alongcoast CTD spacing, by the fact that the CTD station F3 (fortunately) intersected the stagnation streamsurface itself. The approximate slope between 80 and 150 m is estimated to be $\alpha \approx 70$ m/30 km $\approx 5 \times 10^{-3}$. As a consequence, offshore parcels in the upper part of a vertical column of water (denoted by P_U in Fig. 4) intersecting L_{WE} deflect eastward, while lower water parcels (P_L) in the same vertical column of water deflect westward. As a consequence of the motion of P_U and P_L, the horizontal component of the vorticity normal to the vertical plane in Fig. 4 for a water parcel in between P_U and P_L (in the same water column) is positive (i.e., it points north-

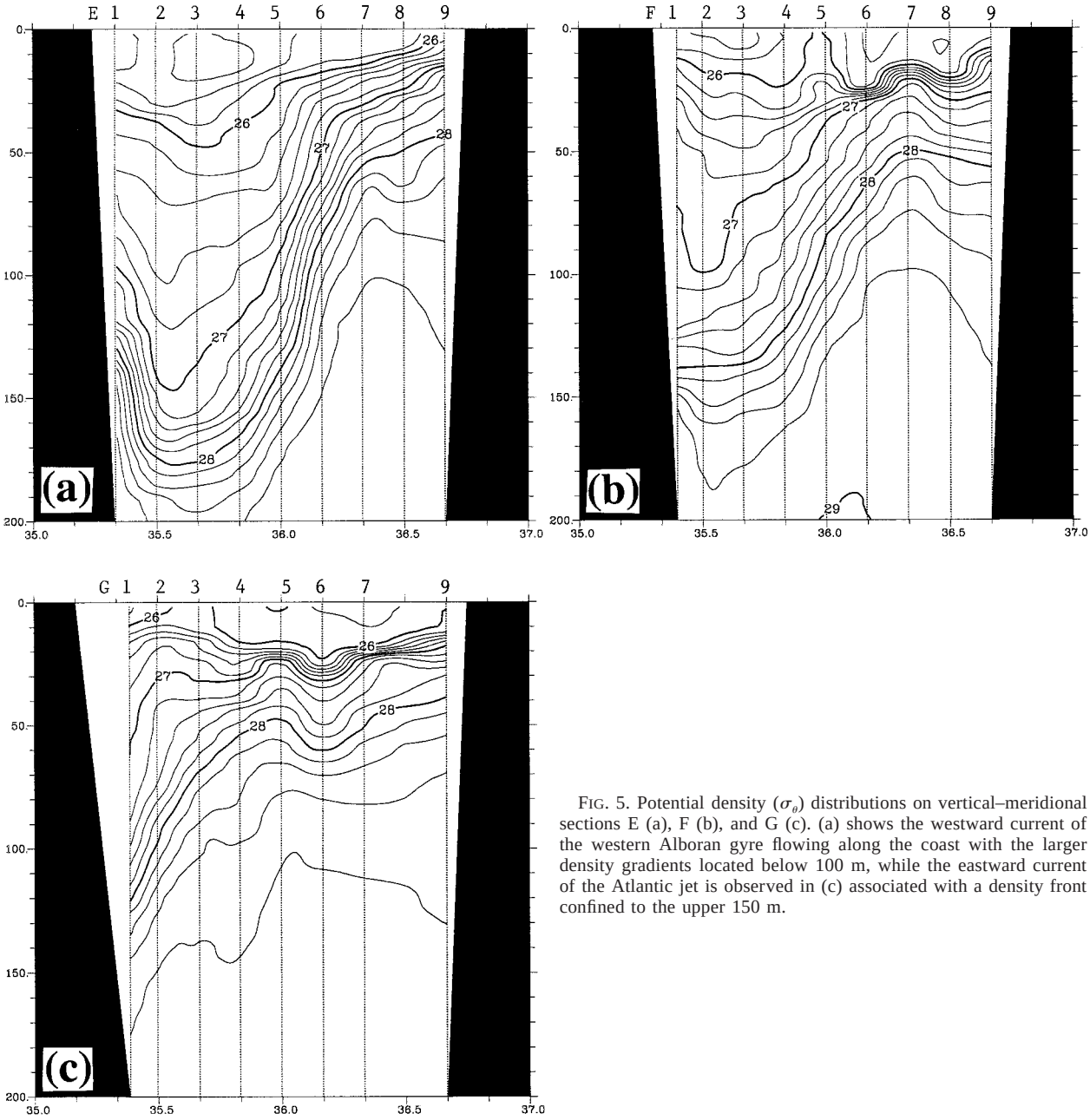

FIG. 5. Potential density (σ_θ) distributions on vertical–meridional sections E (a), F (b), and G (c). (a) shows the westward current of the western Alboran gyre flowing along the coast with the larger density gradients located below 100 m, while the eastward current of the Atlantic jet is observed in (c) associated with a density front confined to the upper 150 m.

ward). Since the impinging current is southward, it is expected that water parcels on the stagnation streamline have negative streamwise vorticity (because the projection of the aforementioned vorticity along the velocity direction is negative).

The hydrographic data can also give us information about the modification of the density field in the AJ as it approaches the coast. Since to a first approximation the circulation can be considered horizontal, the existence of a sloping coast implies that, as a water column approaches the coast, the horizontal distance to the coast is larger for upper water parcels in the column than for lower water parcels. Therefore, changes in the horizontal distance to the coast for vertically separated distributions of potential density (σ_θ), as an approximate conservative property, is a way to infer possible coastal influences. Isolines of σ_θ at different horizontal planes are shown in Fig. 6. The values of σ_θ on each isoline couple correspond to those at four horizontally fixed locations (points A_1 to A_4) at a given depth in the AJ. These results show that the horizontal location of the isolines is approximately constant with depth from points A_1 and A_4 to $\sim 3°40'$W, in such a way that the isolines fit in a narrow band. On the other hand, when

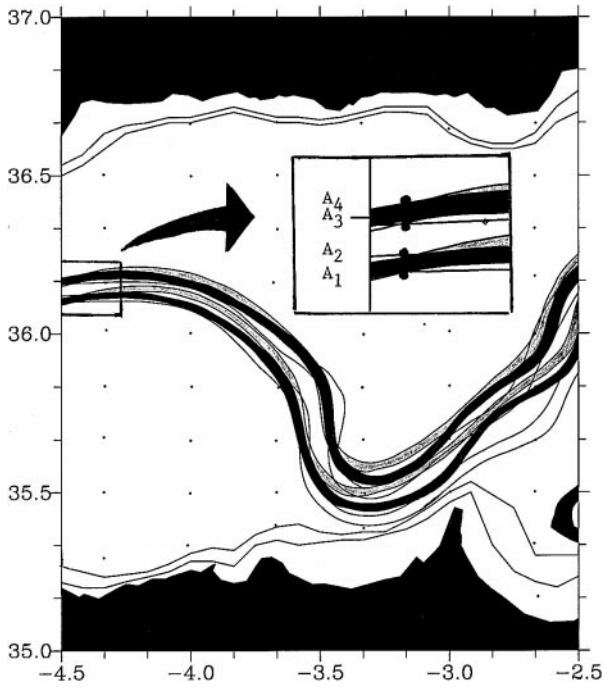

FIG. 6. Isolines of potential density (σ_θ) at different depths (80, 100, and 120 m). The twelve isolines correspond to the values of σ_θ found at points A_1 to A_4 and these are given by (27.52, 27.64, 27.90, 28.03) at 80 m (solid gray); (27.72, 27.86, 28.19, 28.33) at 100 m (black); and (28.03, 28.19, 28.46, 28.59) at 120 m (white).

the AJ curves southward toward the African coast and then turns eastward toward the eastern Alboran basin, the isolines at different depths no longer remain parallel. Potential density isolines in the same water column have, therefore, different orientations. We think this is a consequence of the different horizontal distance to the coast for surface and deep water elements in the AJ, that is, a consequence of the sloping coastal boundary. The kinematical manifestation of all the above features is presented in the next section.

b. Kinematics

In this section we show the main kinematic characteristics of the impinging region based on the vorticity and deformation fields. As part of the density data postprocessing, we obtained an adjusted, dynamically balanced three-dimensional velocity field (Viúdez et al. 1996b) through the dynamical assimilation of the density data into a PE model (Haney 1974, 1985) using the digital filter initialization technique (Lynch and Huang 1992). This method provided a dynamically balanced density and three-dimensional velocity field at the grid points of a $50 \times 40 \times 48$ regular matrix ($\delta x \approx 9.3$ km, $\delta y \approx 6.7$ km, $\delta z = 4$ m) covering the entire Alboran Sea. This assimilation procedure, although not essential for most of the results presented here, provides a more accurate estimate of the velocity field than geostrophic.

The notation used in the remainder of the paper follows that in Gurtin (1981) and Truesdell (1991). We have adopted this notation instead of the Gibbsian dyadic notation (e.g., Morse and Feshbach 1953; Godske et al. 1957; Tai 1992), more common in hydrodynamics, because it is the one most commonly used in continuum mechanics, especially in the study of deformation. In particular a tensor $\mathbf{S}$ is considered to be a linear map that assigns to each vector $\mathbf{b}$ a vector $\mathbf{Sb}$. The spatial gradient, curl, and divergence are denoted as grad, curl, and div. The advective derivative of a vector $\mathbf{b}$ is denoted as (grad $\mathbf{b}$)$\mathbf{v}$, where $\mathbf{v}$ is the velocity field. Directional or intrinsic derivatives of a scalar ϕ or vector-valued function $\mathbf{b}$ in the direction of a unit vector $\mathbf{s}$ are denoted as $\delta\phi/\delta s \equiv \mathbf{s}\cdot\text{grad}\phi$ and $\delta\mathbf{b}/\delta s \equiv$ (grad $\mathbf{b}$)$\mathbf{s}$, respectively. These operators are coordinate independent. Partial derivatives with respect to Cartesian coordinates $\{x_i\}$, $i = 1, 2, 3$, are denoted as $\phi_{,i} \equiv \partial\phi/\partial x_i$. The tensor product $\mathbf{a} \otimes \mathbf{b}$ of two vectors $\mathbf{a}$ and $\mathbf{b}$ is the tensor that assigns to each vector $\mathbf{u}$ the vector $(\mathbf{b}\cdot\mathbf{u})\mathbf{a}$ [that is, $(\mathbf{a} \otimes \mathbf{b})\mathbf{u} = (\mathbf{b}\cdot\mathbf{u})\mathbf{a}$]. Given a Cartesian coordinate frame $\{\mathbf{e}_i\} = \{\mathbf{i}, \mathbf{j}, \mathbf{k}\}$ the components S_{ij} of a tensor $\mathbf{S}$ are defined by $S_{ij} \equiv \mathbf{e}_i\cdot\mathbf{S}\mathbf{e}_j$, so that $\mathbf{S} = S_{ij}\mathbf{e}_i \otimes \mathbf{e}_j$. In particular, grad $\mathbf{a} = a_{i,j}\mathbf{e}_i \otimes \mathbf{e}_j$. Latin indices $i, j, k \in \{1, 2, 3\}$, while Greek indices $\alpha, \beta \in \{1, 2\}$. Summation convection is implicit in repeated indices, except for caret indices (e.g., $\hat{\alpha}\hat{\alpha}$ represents 1 1 or 2 2). The trace is the linear operation satisfying $\text{tr}(\mathbf{a} \otimes \mathbf{b}) = \mathbf{a}\cdot\mathbf{b}$. The transpose $\mathbf{S}^\top$ of $\mathbf{S}$ satisfies $\mathbf{Sa}\cdot\mathbf{b} = \mathbf{a}\cdot\mathbf{S}^\top\mathbf{b}$; in particular $(\mathbf{a} \otimes \mathbf{b})^\top = \mathbf{b} \otimes \mathbf{a}$. The inner product of two tensors $\mathbf{S}$ and $\mathbf{T}$ is defined as $\mathbf{S}\cdot\mathbf{T} \equiv \text{tr}(\mathbf{S}^\top\mathbf{T})$, or in components $\mathbf{S}\cdot\mathbf{T} = S_{ij}T_{ij}$. The magnitude $|\mathbf{S}|$ of the tensor $\mathbf{S}$ is defined as $|\mathbf{S}| \equiv (\mathbf{S}\cdot\mathbf{S})^{1/2}$.

1) CURVATURES AND BACKING

Due to the different scales in the horizontal and vertical components of the velocity field $\mathbf{v}$, let us decompose it into perpendicular horizontal and vertical vectors

$$\mathbf{v}(\mathbf{x}) = \mathbf{v}_h + v_3\mathbf{k}, \qquad \mathbf{v}_h\cdot\mathbf{k} = 0. \tag{1}$$

Defining director vectors for the 3D flow $\mathbf{s}(\mathbf{x}) \equiv \mathbf{v}/v$ (for $v \neq 0$) and for the horizontal flow $\mathbf{s}_h(\mathbf{x}) \equiv \mathbf{v}_h/v_h$ (for $v_h \neq 0$), we have the relation for the director vectors:

$$v\mathbf{s} = v_h\mathbf{s}_h + v_3\mathbf{k}. \tag{2}$$

Let $\mathbf{n}$ and $\mathbf{b}$ be the normal and binormal unit vectors, respectively, of the streamlines of the 3D flow, and $\mathbf{n}_h \equiv \mathbf{k} \times \mathbf{s}_h$ the normal unit vector of the horizontal flow. Then the intrinsic trihedron ($\mathbf{s}$, $\mathbf{n}$, $\mathbf{b}$) and the trihedron ($\mathbf{s}_h$, $\mathbf{n}_h$, $\mathbf{k}$) are a set of orthogonal measuring vectors, in general anholonomic (e.g, see Schouten 1954; Marris and Passman 1968; Goląb 1974, chap. IV), for the 3D flow. The Frenet–Serret-type relations for the vectors ($\mathbf{s}_h$, $\mathbf{n}_h$) are

$$\frac{\delta \mathbf{s}_h}{\delta s_h} = \Theta_S \mathbf{n}_h \qquad \frac{\delta \mathbf{n}_h}{\delta s_h} = -\Theta_S \mathbf{s}_h$$

$$\frac{\delta \mathbf{s}_h}{\delta n_h} = \Theta_N \mathbf{n}_h \qquad \frac{\delta \mathbf{n}_h}{\delta n_h} = -\Theta_N \mathbf{s}_h$$

$$\mathbf{s}_{h,3} = \Theta_Z \mathbf{n}_h \qquad \mathbf{n}_{h,3} = -\Theta_Z \mathbf{s}_h, \tag{3}$$

which may serve as a definition of the streamline curvature of the $\mathbf{s}_h$ and $\mathbf{n}_h$ lines, here denoted Θ_S and Θ_N, respectively, and for the rotation of $\mathbf{s}_h$ along the $\mathbf{k}$ line, or backing, here denoted Θ_Z. The formulas on the rhs of (3) are just a 90° counterclockwise rotation [$\mathbf{k} \times ()$] of the ones on the lhs. Note that curvatures may be computed in an equivalent way from $\Theta_S = \mathbf{k} \cdot \text{curl}\, \mathbf{s}_h$ and $\Theta_N = \mathbf{k} \cdot \text{curl}\, \mathbf{n}_h$. The spatial fields of curvatures and backing for the impinging current are represented in Fig. 7. The streamline curvature field $\Theta_S(\mathbf{x})$, consistent with the pressure anomalies contours, is negative to the right (facing downstream) and positive to the left of the impinging current, where the circulation is anticyclonic and cyclonic, respectively. The curvature of the $\mathbf{n}_h$ lines, Θ_N, can be considered as a measure of the divergence of $\mathbf{s}_h(\mathbf{x})$, or diffluence of the $\mathbf{s}_h$ lines, since $\Theta_N = \mathbf{k} \cdot \text{curl}\, \mathbf{n}_h = \text{div}\, \mathbf{s}_h$. The $\Theta_N(\mathbf{x})$ field shows diffluence ($\Theta_N > 0$) upstream of the impinging region, implying therefore direction divergence ($\upsilon_h \Theta_N > 0$), but confluence ($\Theta_N < 0$) past (i.e., after the flow division) the impinging region, and therefore implying direction convergence ($\upsilon_h \Theta_N < 0$). Since the horizontal flow is almost nondivergent [recall that $\text{div}\, \mathbf{v}_h = \text{div}(\upsilon_h \mathbf{s}_h) = \delta \upsilon_h / \delta s_h + \upsilon_h \Theta_N$], the previous pattern of direction divergence is completed with speed convergence ($\delta \upsilon_h / \delta s_h < 0$) upstream and speed divergence ($\delta \upsilon_h / \delta s_h > 0$) downstream of the impinging region (Fig. 8).

The backing Θ_Z is a measure of the change in direction of the velocity field along the vertical. The backing distribution (Fig. 7c) shows that $\Theta_Z < 0$ upstream far from the impinging region, but $\Theta_Z > 0$ upstream, and $\Theta_Z < 0$ past the stagnation point. Among these different areas characterized by different signs in Θ_Z, probably the most relevant one is where $\Theta_Z < 0$, far upstream, because of the large velocities in the AJ. This importance can be easily visualized by looking at the streamlines at different depths in the AJ (Fig. 9). It is clearly observed how deep streamlines, ''initially'' aligned in the vertical with the surface ones in the AJ, are deflected to the left (facing downstream) ''before'' the surface ones.

In meteorology and oceanography the backing Θ_Z^g of the geostrophic velocity $\mathbf{v}^g$ is important because it represents the advection of density by the geostrophic flow. By defining the vertical shear of the geostrophic velocity through the ''thermal wind'' relation $\mathbf{v}_{,3}^g \equiv -\mathbf{k} \times \text{grad}_h b$ with $b \equiv g\rho(f\rho_o)^{-1}$, and introducing the unit basis vectors ($\mathbf{s}^g$, $\mathbf{n}^g$) for the geostrophic flow, $\mathbf{s}^g \equiv \mathbf{v}^g / \upsilon^g$ and $\mathbf{n}^g \equiv \mathbf{k} \times \mathrm{s}^g$, we find that $\mathbf{v}_{,3}^g = (\upsilon_{,3}^g \mathrm{s}^g)_{,3} = \upsilon_{,3}^g \mathbf{s}^g + \upsilon^g \Theta_Z^g \mathbf{n}^g$, and the $\mathbf{s}^g$ component of the thermal wind relation is $-\upsilon^g \Theta_Z^g = \delta b / \delta s^g$. Therefore $\Theta_Z^g > 0$ implies $\delta b / \delta s^g < 0$. Since the geostrophic advection of b is given by $-\mathbf{v}^g \cdot \text{grad}_h b = -\upsilon^g \delta b / \delta s^g$, the above condition implies positive geostrophic advection of density, or in other words, a decrease of density along the geostrophic streamlines.

2) VORTICITY

In the ($\mathbf{s}$, $\mathbf{n}$, $\mathbf{b}$) reference frame the vorticity is expressed as

$$\boldsymbol{\zeta} \equiv \text{curl}\mathbf{v} = \text{curl}(\upsilon \mathbf{s}) = \text{grad}\upsilon \times \mathbf{s} + \upsilon \text{curl}\mathbf{s}$$
$$= \frac{\delta \upsilon}{\delta b}\mathbf{n} - \frac{\delta \upsilon}{\delta n}\mathbf{b} + \upsilon(\Omega_s \mathbf{s} + \kappa_s \mathbf{b}) \tag{4}$$

(Masotti 1927; Bjørgum 1951), where Ω_s and κ_s, the abnormality and curvature of the $\mathbf{s}$ line, are quantities independent of the magnitude of the velocity field. Note that what is frequently called *secondary vorticity* ($\boldsymbol{\zeta} \cdot \mathbf{s} / \upsilon$) is, in fact, the abnormality Ω_s (e.g., Truesdell and Toupin 1960, p. 386), which is a measure of the departure of $\mathbf{v}$ from the property of having a congruence of surfaces with $\mathbf{s}$ as a normal (e.g., Ericksen 1960, p. 819). In the ($\mathbf{s}_h$, $\mathbf{n}_h$, $\mathbf{k}$) reference frame the relative vorticity may be expressed as

$$\boldsymbol{\zeta} = \text{curl}(\mathbf{v}_h + \upsilon_3 \mathbf{k}) = \boldsymbol{\zeta}_{ph} + \zeta_3 \mathbf{k} + \text{grad}\upsilon_3 \times \mathbf{k}$$
$$= (-\upsilon_h \Theta_Z \mathbf{s}_h + \upsilon_{h,3} \mathbf{n}_h) + \left(\upsilon_h \Theta_S - \frac{\delta \upsilon_h}{\delta n_h}\right)\mathbf{k}$$
$$+ \left(\frac{\delta \upsilon_3}{\delta n_h}\mathbf{s}_h - \frac{\delta \upsilon_3}{\delta s_h}\mathbf{n}_h\right), \tag{5}$$

where $\boldsymbol{\zeta}_{ph}$ is the horizontal component of the pseudovorticity $\boldsymbol{\zeta}_p \equiv \boldsymbol{\zeta}_{ph} + \zeta_3 \mathbf{k}$ (Hoskins 1975; Davies-Jones 1991). Horizontal pseudovorticity is, in fact, a +90° rotation of the vertical shear

$$\mathbf{v}_{h,3} = (\upsilon_h \mathbf{s}_h)_{,3} = \upsilon_{h,3} \mathbf{s}_h + \upsilon_h \Theta_Z \mathbf{n}_h, \tag{6}$$

and then

$$\boldsymbol{\zeta}_{ph} = \mathbf{k} \times \mathbf{v}_{h,3} = -\upsilon_h \Theta_Z \mathbf{s}_h + \upsilon_{h,3} \mathbf{n}_h \tag{7}$$

in the ($\mathbf{s}_h$, $\mathbf{n}_h$) reference frame. In (5) $\boldsymbol{\zeta}$ is decomposed in horizontal pseudovorticity, the vertical component of vorticity ζ_3, and vorticity due to the vertical velocity. The component ζ_3 in (5) is itself decomposed into curvature vorticity ($\upsilon_h \Theta_S$) and shear vorticity ($-\delta \upsilon_h / \delta n_h$).

Relative streamwise vorticity ($\boldsymbol{\zeta} \cdot \mathbf{s}$), or secondary vorticity ($\boldsymbol{\zeta} \cdot \mathbf{s} / \upsilon$), or helicity ($\boldsymbol{\zeta} \cdot \mathbf{v}$), and cross-stream vorticity ($\boldsymbol{\zeta} \cdot \mathbf{n}$), are frequently used in the description of flows (Hawthorne 1951; Hawthorne and Martin 1955; Squire and Winter 1951; Marris 1964; Lakshminarayana and Horlock 1973; Scorer 1978, chap. 3). More recent research dealing with the influence of the cross-stream vorticity of the external flow on the stagnation-point flow and vorticity amplification theory can be found in Sadeh and Brauer (1980) and Dhanak and Stuart (1995).

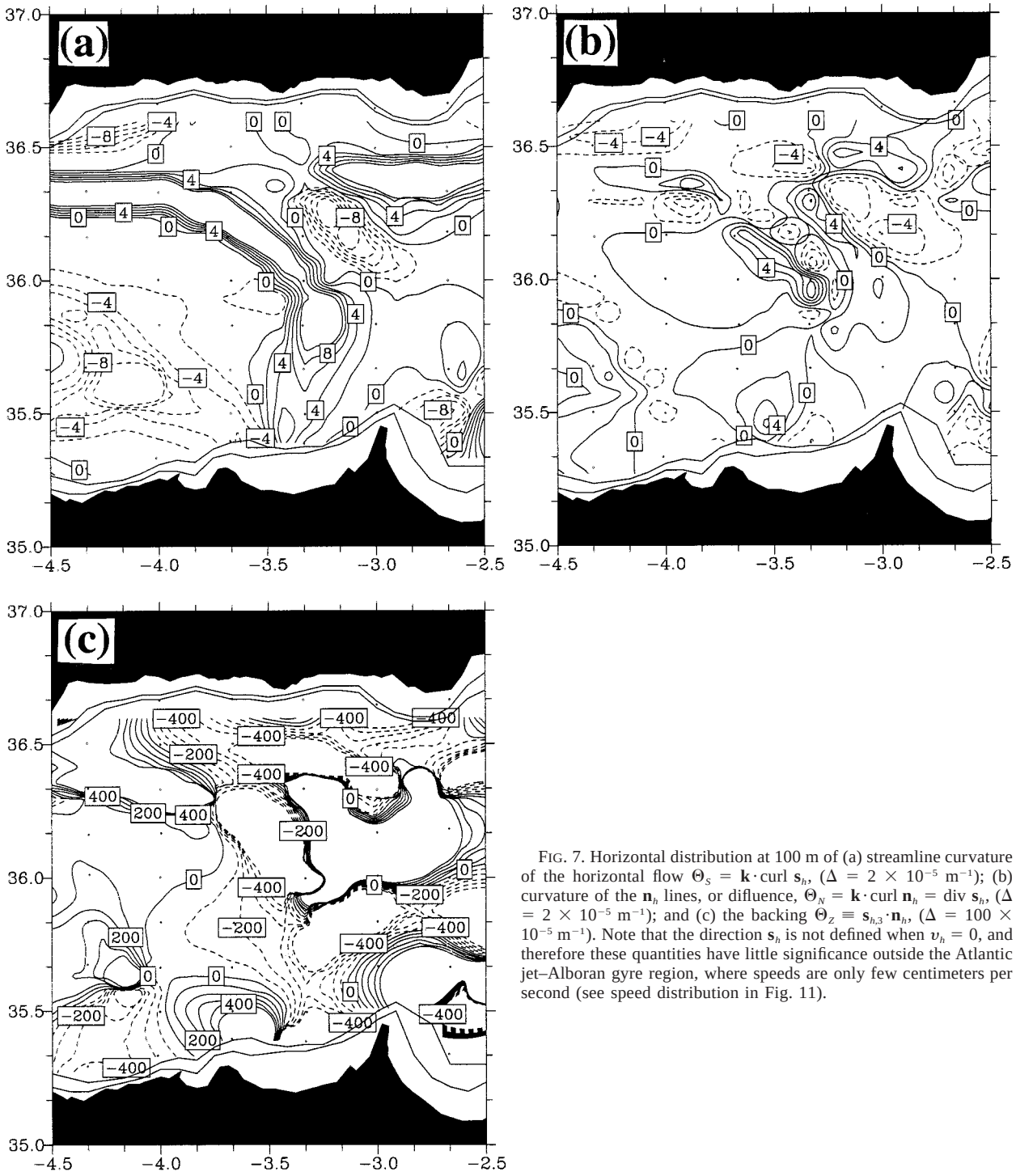

FIG. 7. Horizontal distribution at 100 m of (a) streamline curvature of the horizontal flow $\Theta_S = \mathbf{k}\cdot\text{curl}\,\mathbf{s}_h$, ($\Delta = 2 \times 10^{-5}$ m^{-1}); (b) curvature of the $\mathbf{n}_h$ lines, or difluence, $\Theta_N = \mathbf{k}\cdot\text{curl}\,\mathbf{n}_h = \text{div}\,\mathbf{s}_h$, ($\Delta = 2 \times 10^{-5}$ m^{-1}); and (c) the backing $\Theta_Z \equiv \mathbf{s}_{h3}\cdot\mathbf{n}_h$, ($\Delta = 100 \times 10^{-5}$ m^{-1}). Note that the direction $\mathbf{s}_h$ is not defined when $v_h = 0$, and therefore these quantities have little significance outside the Atlantic jet–Alboran gyre region, where speeds are only few centimeters per second (see speed distribution in Fig. 11).

The explicit use of streamwise vorticity in the study of atmospheric or oceanic phenomena appears to be more limited. However, since streamwise vorticity is closely related to the backing/veering of $\mathbf{v}_h$ along $\mathbf{k}$, it has received, at least implicitly, considerable attention in both atmospheric and oceanic processes. Scorer and Wilson (1963) uses it to study the instability in atmospheric gravity waves. Davies-Jones (1984) and Brandes et al. (1988) consider the storm-relative streamwise vorticity to play a main role in the origin of organized rotation in supercell storms. Evidently, none of the above quantities [$\boldsymbol{\zeta}\cdot\mathbf{s}$, $\boldsymbol{\zeta}\cdot\mathbf{n}$, $\boldsymbol{\zeta}\cdot\mathbf{s}/v$, $\boldsymbol{\zeta}\cdot\mathbf{v}$, mean helicity $\langle\boldsymbol{\zeta}\cdot\mathbf{v}\rangle$ (Speziale

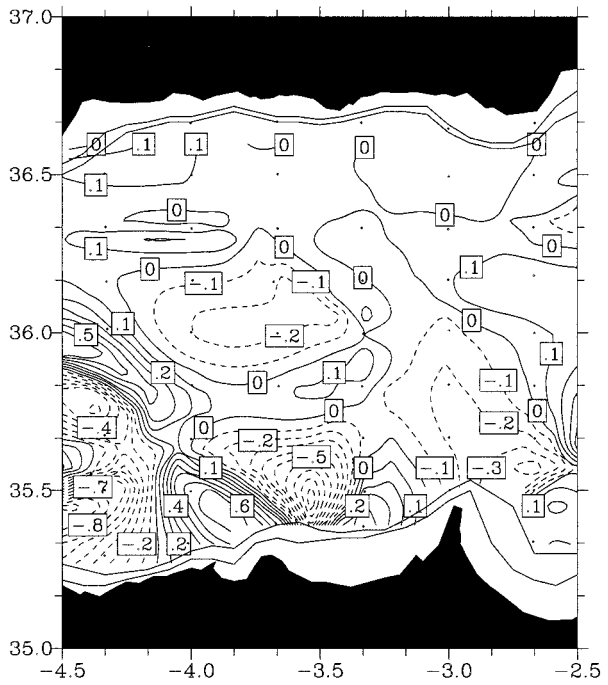

FIG. 8. Horizontal distribution at 100 m of speed-divergence $\delta v_h/\delta s_h$, ($\Delta = 0.1$ s^{-1}). Note that since div $\mathbf{v}_h \approx 0$, this distribution is very close to minus the directional divergence distribution $v_h\Theta_N$.

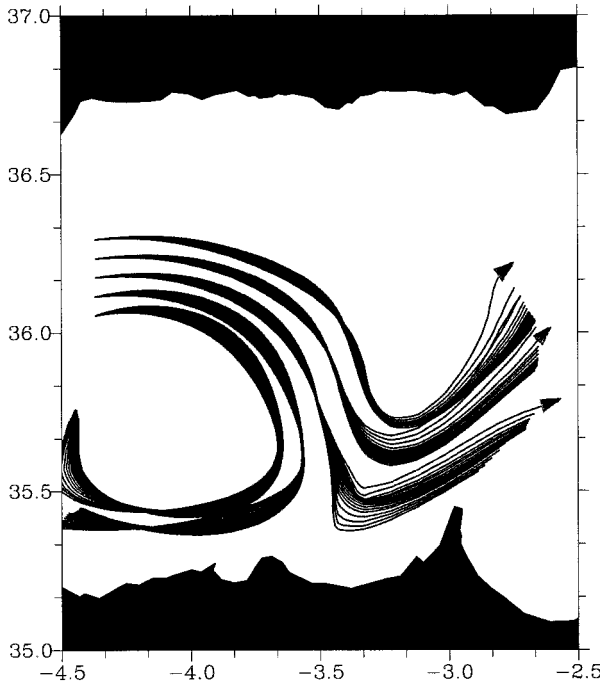

FIG. 9. Top view, or horizontal projection, of five streamline sets corresponding to the impinging current. There are 26 streamlines in each set, all *beginning* at the same horizontal location and separated by 4 m in the vertical, from 18 m to 118 m depth. All streamlines are 200 km long. The deepest streamlines of the Atlantic jet are those having an arrow.

1987), etc.] are Galilean invariant. In Brandes et al. (1988) it is argued that only streamwise vorticity relative to the reference system in which the storm is steady has physical significance. On the other hand, most of the previous studies deal with steady-state circulation, which also is not a Galilean invariant concept, and therefore they also assume a preferred reference frame (precisely, the reference frame in which the flow is steady). Dealing also with boundary interaction processes there is also a preferred reference system, that is, that in which the boundary is at rest. This is implicitly assumed when the motion is referred to rotating (fixed to the earth) coordinate axes. Therefore, streamwise vorticity can be considered a suitable quantity in the kinematic description of impinging jet processes. Using (2) and (5) the streamwise relative vorticity can be written as

$$\boldsymbol{\zeta}\cdot\mathbf{s} = (\boldsymbol{\zeta}_{ph} + \zeta_3\mathbf{k} + \text{grad}v_3 \times \mathbf{k})\cdot(v_h\mathbf{s}_h + v_3\mathbf{k})v^{-1}$$

$$= \frac{v_h}{v}\boldsymbol{\zeta}_{ph}\cdot\mathbf{s}_h + \frac{v_h}{v}\frac{\delta v_3}{\delta n_h} + \frac{v_3}{v}\zeta_3. \tag{8}$$

Since $v_3/v = O(10^{-3})$ the analysis of streamwise vorticity $\boldsymbol{\zeta}\cdot\mathbf{s} = v\Omega_s$ is, to a good approximation, the analysis of the component of the horizontal pseudovorticity in the direction of the horizontal flow $\boldsymbol{\zeta}_{ph}\cdot\mathbf{s}_h = -v_h\Theta_Z$. On the other hand, the $\mathbf{n}_h$ component of the vorticity

$$\boldsymbol{\zeta}\cdot\mathbf{n}_h = v_{h,3} - \frac{\delta v_3}{\delta s_h} \tag{9}$$

is approximately the $\mathbf{n}_h$ component of the pseudovorticity, which from (7) is the vertical derivative of the horizontal speed $\boldsymbol{\zeta}_{ph}\cdot\mathbf{n}_h = v_{h,3}$. The vorticity components in the ($\mathbf{s}_h$, $\mathbf{n}_h$, $\mathbf{k}$) directions for the impinging current are shown in Fig. 10. It is observed that cross-stream vorticity experiences a large decrease from 500 to 200 ($\times 10^{-5}$ s^{-1}) when the impinging current approaches the coast. The vertical component ζ_3, having contours quite parallel to the isobars, is relatively conserved along streamlines in the impinging area. Note that $(\boldsymbol{\zeta}_{ph}\cdot\mathbf{n}_h)/\zeta_3 = O(5 \times 10^2)$. Streamwise vorticity, however, decreases from ~ 0 to -150×10^{-5} s^{-1} as the current approaches the coast. Streamwise vorticity of a water parcel is therefore the only vorticity component that, in spite of the decrease in speed (Fig. 11), increases in magnitude as the fluid element impinges on the coast. As a water parcel approaches the coast the horizontal pseudovorticity $\boldsymbol{\zeta}_{ph}$, initially almost pointing eastward, experiences a large contraction together with a counterclockwise rotation in such a way that the magnitude of the streamwise vorticity becomes comparable to the magnitude of the cross-stream vorticity. Since $\boldsymbol{\zeta}_{ph}\cdot\mathbf{s}_h = -v_h\Theta_Z$, veering ($\Theta_Z < 0$, clockwise rotation of $\mathbf{v}_h$ with $\mathbf{k}$) always implies positive streamwise pseudovorticity, and, conversely, backing ($\Theta_Z < 0$, counterclockwise rotation of $\mathbf{v}_h$ with $\mathbf{k}$) always implies negative streamwise pseudovorticity. In steady state, and neglecting vertical advection, the material derivative of $\boldsymbol{\zeta}_{ph}\cdot\mathbf{s}_h$ is given by the horizontal alongstream derivative of $\boldsymbol{\zeta}_{ph}\cdot\mathbf{s}_h$,

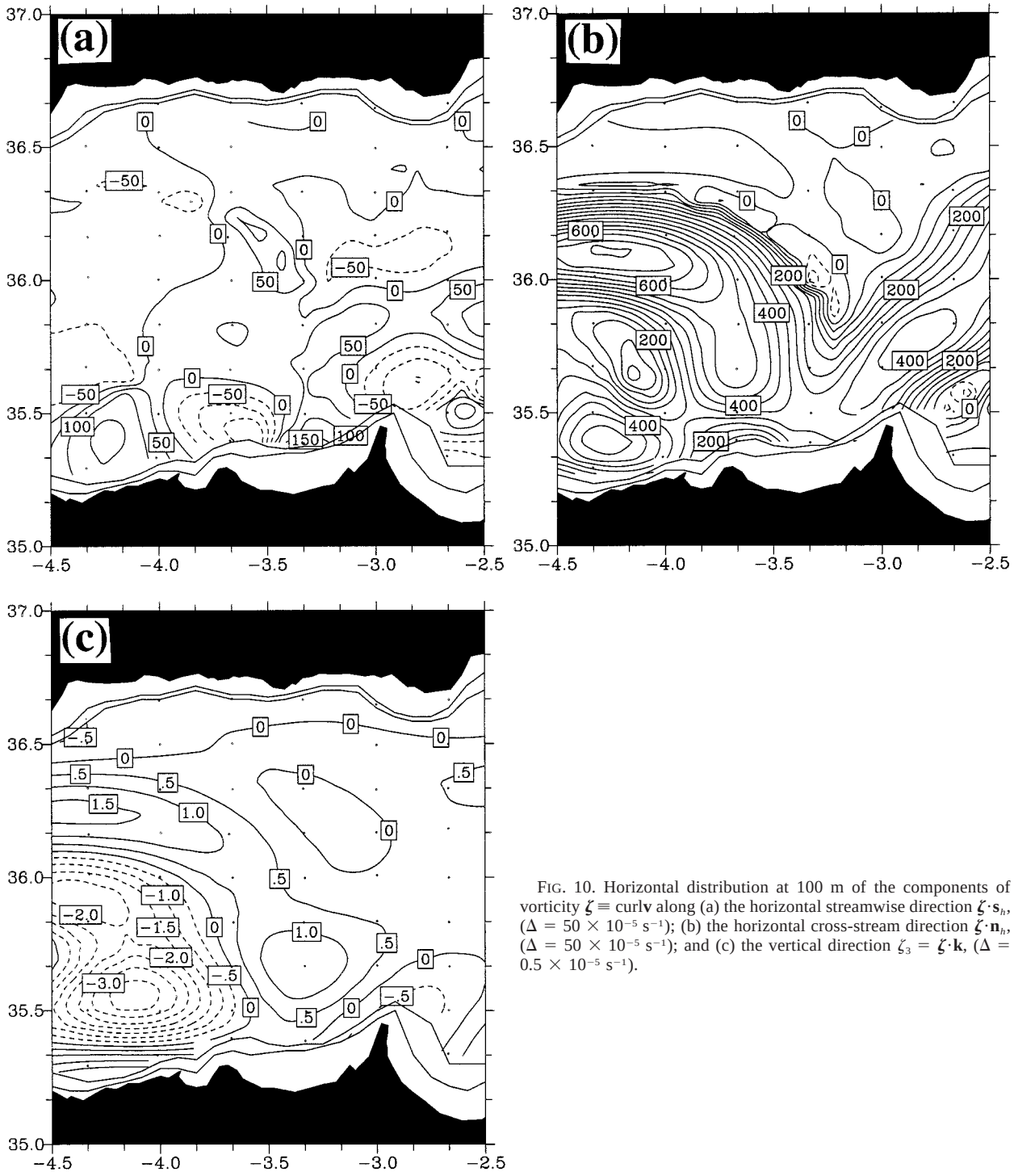

FIG. 10. Horizontal distribution at 100 m of the components of vorticity $\boldsymbol{\zeta} \equiv \text{curl}\mathbf{v}$ along (a) the horizontal streamwise direction $\boldsymbol{\zeta}\cdot\mathbf{s}_h$, ($\Delta = 50 \times 10^{-5}$ s^{-1}); (b) the horizontal cross-stream direction $\boldsymbol{\zeta}\cdot\mathbf{n}_h$, ($\Delta = 50 \times 10^{-5}$ s^{-1}); and (c) the vertical direction $\zeta_3 = \boldsymbol{\zeta}\cdot\mathbf{k}$, ($\Delta = 0.5 \times 10^{-5}$ s^{-1}).

$$\frac{\delta}{\delta s_h}(-v_h\Theta_Z) = -\frac{\delta v_h}{\delta s_h}\Theta_Z - \frac{\delta\Theta_Z}{\delta s_h}v_h, \qquad (10)$$

which states that a decrease of negative $\zeta_{ph}\cdot\mathbf{s}_h$ ($\Theta_Z > 0$) along streamlines may be due to a speed divergence ($\delta v_h/\delta s_h > 0$) or to a streamwise increase of the backing Θ_Z. Since the region upstream of the stagnation point is characterized by speed convergence ($\delta v_h/\delta s_h < 0$), there is a steady decrease of $\zeta_{ph}\cdot\mathbf{s}_h$ when there is a streamwise increase in the backing ($\delta\Theta_Z/\delta s_h$) and when this increase in backing is such that $v_h\delta\Theta_Z/\delta s_h > -\Theta_Z\delta v_h/\delta s_h$. The streamwise increase of the backing

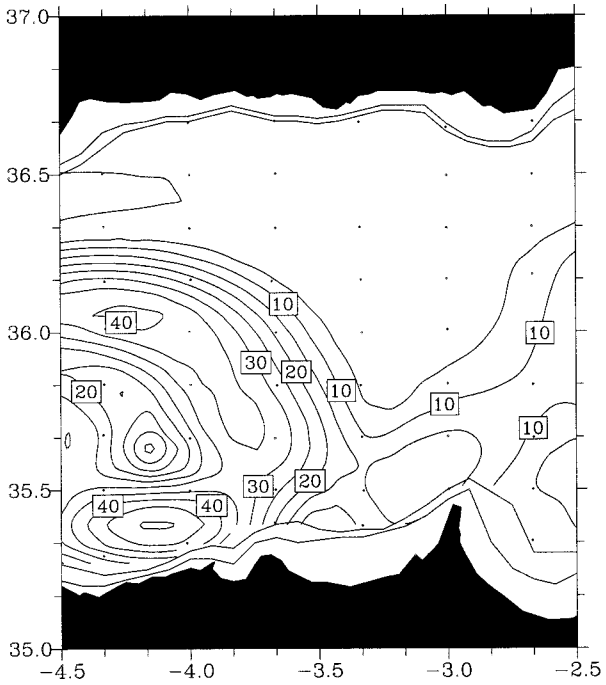

FIG. 11. Horizontal distribution at 100 m of the speed $v \equiv \|\mathbf{v}\|$, ($\Delta = 5 \times 10^{-2}$ m s^{-1}).

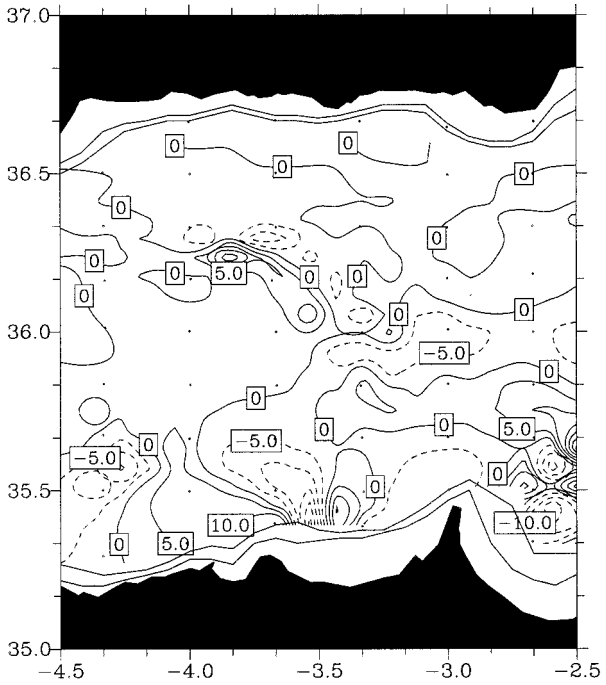

FIG. 12. Horizontal distribution at 100 m of the streamwise changes in horizontal pseudovorticity due to the streamwise changes of backing ($-v_h \delta\Theta_Z/\delta s_h$), ($\Delta = 5 \times 10^{-8}$ m^{-1} s^{-1}).

upstream of the stagnation area can be easily deduced from the Θ_Z distribution (Fig. 7c). The corresponding distribution of $-v_h \delta\Theta_Z/\delta s_h$ (Fig. 12) shows that the alongstream changes in $\boldsymbol{\zeta}_{ph} \cdot \mathbf{s}_h$ are, in fact, due to the changes in the backing. The distribution of $-\Theta_Z \delta v_h/\delta s_h$ (not shown) has positive values upstream of the stagnation area (because $\Theta_Z > 0$ and $\delta v_h/\delta s_h < 0$) but these values are negligible with respect to the values of $-v_h \delta\Theta_Z/\delta s_h$. These distributions show, therefore, that the streamwise changes in the horizontal pseudovorticity are, in fact, due to the corresponding streamwise changes in backing.

The kinematic properties presented above are significant for several reasons. First, they represent a quantitative description of the three-dimensional velocity field in the impinging region. As such, they provide quantitative and meanful data for testing theories or models of the impinging process. One could, in principle, have done this description directly by simply mapping the velocity at different levels. Such a method, however, would be largely imprecise and only qualitative in nature. From the already mentioned non-Galilean invariance of these kinematic quantities, it is clear that they have no dynamical significance. Since the impinging jet is characterized by large changes of opposite sign in speed divergence and direction divergence (the changes in horizontal divergence can be neglected in comparison with the changes in speed divergence or direction divergence), the impinging process could be considered a very good example of a conversion between speed divergence and direction divergence and be studied using the interchange equations proposed by Hollmann (1958). However, such a treatment would also be considered a description and not an explanation of the changes in speed divergence and direction divergence (see equivalent conclusions regarding the shear and curvature vorticity equations in Viúdez and Haney 1996). The kinematic quantities presented above are also important because of their connection to certain experimental methods. For example, a satellite thermal image may be used to infer the streamline curvature field but, in general, not the velocity field. From the trajectory of a single isopycnal float we can measure the curvature vorticity, but not vorticity itself. We will see in the next two sections that many of the properties of the velocity field in this study, including the deformation, can be deduced from the single fact that the acceleration field is divergent in the impinging region.

3) ROTATION AND DEFORMATION

The previous remarks have shown that the relative vorticity of a water parcel in the impinging current experiences notable changes as it approaches the African coast. However, since any continuous motion at a given instant of time is composed of a translation, a rigid rotation, and a pure deformation, it becomes equally important to determine the relative significance of the deformation field in the stagnation current. A measure of the ratio of the magnitude of rotation to the magnitude of deformation was introduced by Truesdell (1953,

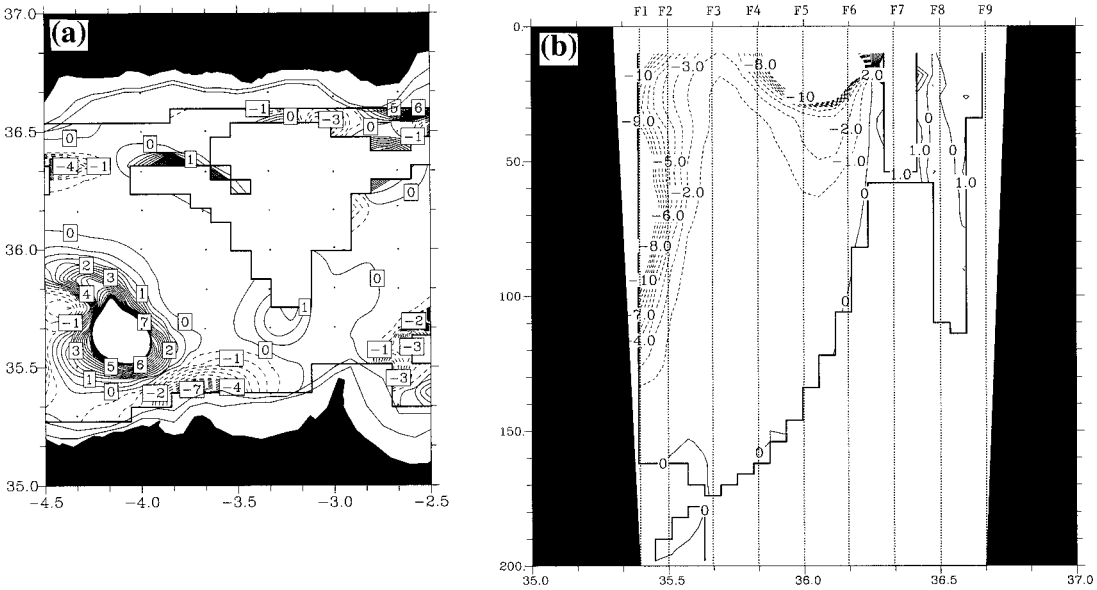

FIG. 13. Horizontal distribution (a) at 100 m and vertical distribution (b) along section F of $(W_K - 1) \times 10^{-5}$, where W_K is the kinematical vorticity number. Positive values indicate $W_K > 1$. Contours range from -10 to 10 with $\Delta = 0.5$. Interior areas where $v < 2$ cm s^{-1} are assumed to have large numerical errors and have been blanked.

1954) by defining the *kinematical vorticity number* as the dimensionless scalar

$$W_K \equiv \frac{|\mathbf{W}|}{|\mathbf{D}|}, \tag{11}$$

where $\mathbf{D}$ and $\mathbf{W}$ are the symmetric and skew-symmetric parts of the velocity gradient (the *stretching* and *spin* tensors, respectively)

$$\mathbf{L} \equiv \text{grad}\mathbf{v} = \frac{1}{2}(\mathbf{L} + \mathbf{L}^{\mathrm{T}}) + \frac{1}{2}(\mathbf{L} - \mathbf{L}^{\mathrm{T}}) = \mathbf{D} + \mathbf{W}. \tag{12}$$

Note that $|\mathbf{W}|^2 = \mathbf{W}\cdot\mathbf{W} = W_{ij}W_{ij} = (1/2)\zeta^2$, where $\zeta \equiv \|\text{curl } \mathbf{v}\|$ is the magnitude of the relative vorticity. Since a rigid rotation has $D_{ij} = 0$, $\zeta \neq 0$, and a nonrigid irrotational motion has $\zeta = 0$, $\mathbf{D}\cdot\mathbf{D} \neq 0$, the kinematical vorticity number provides a numerical degree of rotationality for all possible motions (exception are the rigid translations) on a scale from 0 (rigid rotational motion) to ∞ (nonrigid irrotational motion). When $W_K = 1$, spin and stretching are precisely balanced. Since

$$\mathbf{L}\cdot\mathbf{L}^{\mathrm{T}} = (\mathbf{D} + \mathbf{W})\cdot(\mathbf{D} + \mathbf{W})^{\mathrm{T}} = \mathbf{D}\cdot\mathbf{D} - \mathbf{W}\cdot\mathbf{W}, \tag{13}$$

we have

$$|\mathbf{D}|^2 = \frac{1}{2}\zeta^2 + \mathbf{L}\cdot\mathbf{L}^{\mathrm{T}}, \tag{14}$$

and therefore from (11)

$$W_K = \left(1 + \frac{2\mathbf{L}\cdot\mathbf{L}^{\mathrm{T}}}{\zeta^2}\right)^{-1/2}. \tag{15}$$

Since in the impinging current $(1/2)\zeta^2 = O(10^{-5}\ \text{s}^{-2})$ and $\mathbf{L}\cdot\mathbf{L}^{\mathrm{T}} = O(10^{-10}\ \text{s}^{-2})$ at, say 100 m, the kinematical vorticity number is $W_K = 1 \pm O(10^{-5})$. The W_K distribution is shown in Fig. 13 as $(W_K - 1) \times 10^5$. It is observed that, while the magnitude of rotation is larger than the magnitude of deformation in the WAG ($W_K > 1$), the magnitude of deformation exceeds the magnitude of rotation when the current impinges on the African coast ($W_K < 1$). Note that in the impinging region $W_K \ll 0$ from the surface to ~150 m, while in the AJ this only occurs in the surface (from 0 to 50 m) layer. Because of this clear signature, deformation is a very important quantity in the kinematic description of impinging jet processes. Since ζ^2 is a positive quantity, the positive or negative departure of W_K from 1 depends on the sign of $\mathbf{L}\cdot\mathbf{L}^{\mathrm{T}}$. If $\mathbf{L}\cdot\mathbf{L}^{\mathrm{T}} > 0$ then $W_K < 1$. The quantity $\mathbf{L}\cdot\mathbf{L}^{\mathrm{T}} = L_{ij}L_{ji} = v_{i,j}v_{j,i}$ at 100 m is shown in Fig. 14. It exhibits positive values in the impinging area and negative values in the WAG area, according to the W_K distribution. The fact that we are considering nondivergent motions (div $\mathbf{v} = 0$) allows us to give an alternative kinematic interpretation of the term $\mathbf{L}\cdot\mathbf{L}^{\mathrm{T}}$. By taking the divergence of the advective derivative $\mathbf{Lv}$ we have

$$\text{div}(\mathbf{Lv}) = [\text{grad}(\text{div } \mathbf{v})]\cdot\mathbf{v} + \mathbf{L}\cdot\mathbf{L}^{\mathrm{T}}, \tag{16}$$

or in Cartesian components

$$(v_{i,j}v_j)_{,i} = v_{i,ji}v_j + v_{i,j}v_{j,i}. \tag{17}$$

The first term on the right-hand side is zero since div $\mathbf{v} = v_{i,i} = 0$. Therefore, $\mathbf{L}\cdot\mathbf{L}^{\mathrm{T}}$ represents the divergence of the advective derivative of $\mathbf{v}$ for nondivergent motions. Since the acceleration field $\mathbf{a} = \mathbf{v}_{,t} + \mathbf{Lv}$, the term $\mathbf{L}\cdot\mathbf{L}^{\mathrm{T}}$ also represents the divergence of the acceleration field (div $\mathbf{a}$) for steady flows ($\mathbf{v}_{,t} = \mathbf{0}$). Since $(\mathbf{a}\cdot\mathbf{k})_{,3}$ is

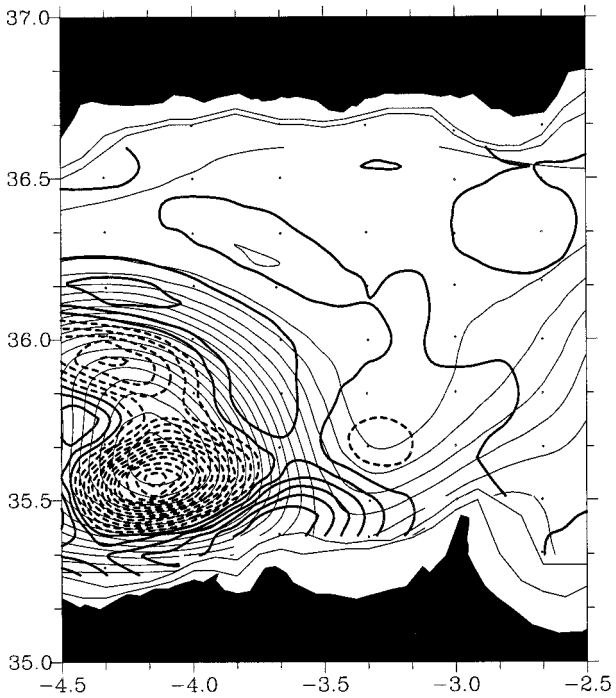

FIG. 14. Horizontal distribution of $\mathbf{L}\cdot\mathbf{L}^{\mathrm{T}}$ (thick isolines) at 100 m. Continuous isolines indicate positive or zero contour values ($\Delta = 0.5 \times 10^{-10}$ s^{-2}). Thin isolines represent pressure anomalies.

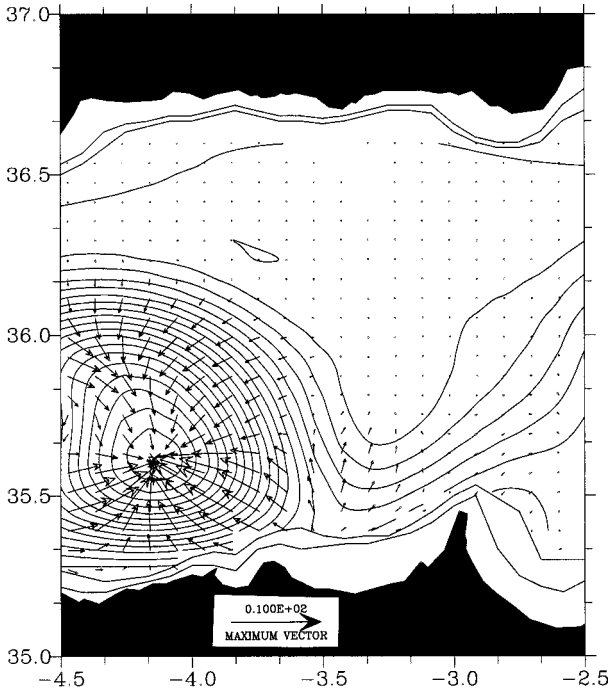

FIG. 15. Advective derivative of $\mathbf{v}_h$ at 100 m. Reference vector is 10^{-5} m s^{-2}. Thin isolines represent pressure anomalies.

negligible for hydrostatic flows, we have for nondivergent hydrostatic steady flows div $\mathbf{a} \approx$ div $\mathbf{a}_h =$ div(grad $\mathbf{v}_h$)$\mathbf{v}$, where grad $\mathbf{v}_h = v_{\alpha,i}\,\mathbf{e}_\alpha \otimes \mathbf{e}_i$. The advective derivative of $\mathbf{v}_h$ is shown in Fig. 15. Besides the centripetal acceleration of the fluid elements in the WAG circulation directed toward its center, the deceleration of the current before impinging on the coast ($\mathbf{a}_h$ vectors are opposite to the flow direction) and the tendency of the flow to accelerate after the flow division ($\mathbf{a}_h$ vectors have a positive component in the direction of the flow) are also clearly observed. In the steady state, this deceleration–acceleration of the fluid produces the divergence of $\mathbf{a}_h$ (div $\mathbf{a}_h > 0$), which implies $\mathbf{L}\cdot\mathbf{L}^{\mathrm{T}} > 0$ and therefore $W_K < 1$.

It should be noted that, as it is usual practice in oceanography, the velocity field used in the computation of W_K is referenced to the rotating earth. Thus, W_K is in fact a relative vorticity number. If velocity is instead referenced to a nonrotating system absolute vorticity should replace the relative vorticity in (11). The *absolute* vorticity number so obtained is one order of magnitude larger than the relative W_K and is always positive in the study domain, with a relative extremum, in this case a maximum, in the impinging region. This shows the large effect that the solid (nondeformable) coastal boundaries have in communicating their own rotation to the oceanic flow.

Separation between horizontal and vertical velocity components for the term $\mathbf{L}\cdot\mathbf{L}^{\mathrm{T}}$ may be clarified by using (1) to write

$$\mathbf{L} \equiv \mathrm{grad}\mathbf{v} = \mathrm{grad}\mathbf{v}_h + \mathrm{grad}(v_3\mathbf{k})$$

$$= \mathrm{grad}_h\mathbf{v}_h + \mathbf{v}_{h,3} \otimes \mathbf{k} + \mathbf{k} \otimes \mathrm{grad}v_3. \quad (18)$$

Defining $\mathbf{L}_h = \mathrm{grad}_h\mathbf{v}_h \equiv v_{\alpha,\beta}\mathbf{e}_\alpha \otimes \mathbf{e}_\beta$ and using the identity $(\mathbf{a} \otimes \mathbf{b})\cdot(\mathbf{c} \otimes \mathbf{d}) = \mathbf{a}\cdot\mathbf{c}\,\mathbf{b}\cdot\mathbf{d}$, we obtain

$$\mathbf{L}\cdot\mathbf{L}^{\mathrm{T}} = \mathbf{L}_h\cdot\mathbf{L}_h^{\mathrm{T}} + 2\mathbf{v}_{h,3}\cdot\mathrm{grad}\,v_3 + v_{3,3}^2. \quad (19)$$

The horizontal version of (16) is

$$\mathrm{div}(\mathbf{L}_h\,\mathbf{v}_h) = [\mathrm{grad}(\mathrm{div}\,\mathbf{v}_h)]\cdot\mathbf{v}_h + \mathbf{L}_h\cdot\mathbf{L}_h^{\mathrm{T}}, \quad (20)$$

using div $\mathbf{v}_h = -v_{3,3}$, and moving $\mathbf{L}_h\cdot\mathbf{L}_h^{\mathrm{T}}$ to the lhs, we get

$$\mathbf{L}_h\cdot\mathbf{L}_h^{\mathrm{T}} = \mathrm{div}(\mathbf{L}_h\mathbf{v}_h) + \mathbf{v}_h\cdot\mathrm{grad}\,v_{3,3}. \quad (21)$$

Thus, $\mathbf{L}_h\cdot\mathbf{L}_h^{\mathrm{T}}$ represents the horizontal divergence of the horizontal advective derivative of $\mathbf{v}_h$ when the flow is horizontal and nondivergent. Note also that, if $v_3 = 0$, then by (19) $\mathbf{L}\cdot\mathbf{L}^{\mathrm{T}} = \mathbf{L}_h\cdot\mathbf{L}_h^{\mathrm{T}}$. These results have to be taken into account since in our study $v_3/v_h = (10^{-3})$. Therefore, the distributions of $\mathbf{L}\cdot\mathbf{L}^{\mathrm{T}}$ in the impinging current (Fig. 14) and div($\mathbf{L}_h\mathbf{v}_h$) are mainly due to the horizontal flow $\mathbf{v}_h$ since $\mathbf{L}\cdot\mathbf{L}^{\mathrm{T}} \approx \mathbf{L}_h\cdot\mathbf{L}_h^{\mathrm{T}} \approx$ div($\mathbf{L}_h\mathbf{v}_h$) when $v_3/v_h \ll 1$.

4) STRETCHING

The study of stretching may be accomplished by means of the principal stretchings and principal axes of stretching. The reader is referred to Chadwick (1976), Gurtin (1981), and Truesdell (1991) for a detailed exposition of these topics. The principal stretchings are

the proper numbers of the symmetric tensor $\mathbf{D}$. Briefly, and practically quoting Chadwick (1976, p. 75–76), since $\mathbf{D}$ is a symmetric tensor, it possesses three proper numbers called the principal stretchings, and an orthogonal triad of proper vectors $\mathbf{d}_k(\mathbf{x}, t)$, $k = 1, 2, 3$ whose directions are called the principal axes of stretching. The principal stretchings (at a point $\mathbf{x}$) are the rates of extension per unit length experienced by material line elements currently aligned with the principal axes of stretching. Moreover, the rates of change of the angles between these lines are momentarily zero. Material elements along these principal axes of stretching are instantaneously suffering no rotation with respect to one another. Their motion as lines, no account being taken of the motion of particles along them, is instantaneously rigid; hence the spin is the angular velocity of the principal axes of stretching, in the ordinary sense of rigid motions (Truesdell and Toupin 1960, p. 355). The relative motion in the vicinity of the point $\mathbf{x}$ consists of a triaxial stretching, represented by $\mathbf{D}$, superimposed upon a rigid rotation specified by $\mathbf{W}$. Since it can be shown that the stretching tensor $\mathbf{D}$ is dominated by the large values of $\mathbf{v}_{h,3}$, a direct representation of the stretching axes of the 3D flow is, in general, unsuitable (see the appendix).

We may instead consider the deformation of the horizontal two-dimensional flow. In this representation the 3D flow is thought to be composed of a set of 2D horizontal layers, and vertical motion is not considered. In this description every layer is two-dimensional and is treated from a kinematic point of view as an independent material system. The corresponding velocity gradient is $\mathbf{L}_h$ (see the appendix for symbol definitions) and the stretching tensor is $\mathbf{D}_h$. The proper unit vectors $\mathbf{c}_\alpha$ and the proper values λ_α satisfy

$$\mathbf{D}_h\mathbf{c}_\alpha = \lambda_{\hat{\alpha}}\mathbf{c}_{\hat{\alpha}}. \tag{22}$$

The spectral decomposition of $\mathbf{D}_h$ is $\mathbf{D}_h = \lambda_\alpha\mathbf{c}_\alpha \otimes \mathbf{c}_\alpha$. Since div $\mathbf{v}$ = div $\mathbf{v}_h + v_{3,3} = 0$, then div $\mathbf{v}_h = \text{tr}(\mathbf{D}_h) = \Sigma\,\lambda_\alpha = -v_{3,3}$. But $v_{3,3}/v_h = O(10^{-3})$ and therefore the proper values λ_α are to a large extent equal in magnitude but opposite in sign. The spatial field of proper vectors $\mathbf{c}_\alpha$ in the impinging current is shown in Fig. 16. The direction of these vectors indicates therefore the stretching axes of the horizontal 2D flow. Since the sense of the vectors is irrelevant ($-\mathbf{c}_\alpha$ are also proper vectors), we have adopted the convention of representing the vector $\pm\lambda_{\hat{\alpha}}\mathbf{c}_{\hat{\alpha}}$ satisfying that sgn$(\pm\lambda_{\hat{\alpha}}\mathbf{c}_{\hat{\alpha}}\cdot\mathbf{v}_h)$ is equal to sgn(λ_α). Therefore, in Fig. 16 when $\lambda_{\hat{\alpha}}\mathbf{c}_{\hat{\alpha}}$ is in the direction of $\mathbf{v}_h$, there is positive stretching ($\lambda_\alpha > 0$) in that direction. It is observed that the stretching axes $\pm\mathbf{c}_\alpha$ of the current before impinging on the coast form an approximately 45° angle with the flow. Therefore, the magnitude of rotation equals the magnitude of deformation, a result already observed from the kinematical vorticity number distribution. As a water parcel in the current approaches the coast (we are assuming steady state in this description) a rotation (relative to the flow direction) of its stretching axes occurs in such a way that the axes become almost parallel and normal to the coast in the impinging region. There occurs an enhancement of the stretching, with positive stretching in the direction parallel to the coast and negative stretching in the direction normal to the coast.

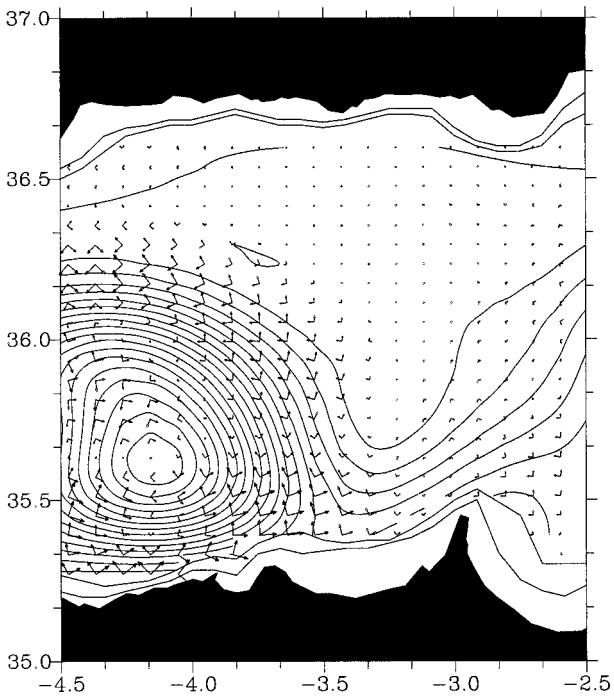

FIG. 16. Distribution at 100 m of the stretchings $\mathbf{D}_h\mathbf{c}_\alpha = \lambda_{\hat{\alpha}}\mathbf{c}_{\hat{\alpha}}$ ($\alpha = 1, 2$). We have represented only one of the two vectors $\pm\lambda_{\hat{\alpha}}\mathbf{c}_{\hat{\alpha}}$ [the one satisfying sign$(\pm\lambda_{\hat{\alpha}}\mathbf{c}_{\hat{\alpha}}\cdot\mathbf{v}_h)$ = sign$(\lambda_{\hat{\alpha}})$]. Thin isolines represent pressure anomalies.

3. Discussion and conclusions

The results concerning the impinging process may be summarized by the sketch in Fig. 17. In the horizontal we distinguish between several areas labeled from I to IV. The first area (I) is upstream, far from the impinging region. In this area the horizontal flow is not normal to the coast, the stagnation streamlines have relatively large horizontal curvature, and the backing is negative ($\Theta_Z < 0$). When the flow approaches the coast and arrives at the impinging region proper, there is an upstream impinging region (area II) where the flow has speed convergence ($\delta v_h/\delta_h < 0$), and therefore diffluence ($\Theta_N > 0$) and speed deceleration ($\mathrm{d}v_h/\mathrm{d}t \approx v_h\delta v_h/\delta s_h < 0$ in the steady state). This region is characterized by positive backing ($\Theta_Z > 0$) and, therefore, by negative streamwise pseudovorticity ($-v_h\Theta_Z < 0$). Past the impinging region, the two horizontal flow branches (areas III and IV) experience speed divergence ($\delta v_h/\delta s_h > \mathrm{O}$), therefore confluence ($\Theta_N < 0$) and speed acceleration ($\mathrm{d}v_h/\mathrm{d}t \approx v_h\delta v_h/\delta s_h > 0$ in the steady state). These two areas (III and IV) are characterized by negative backing

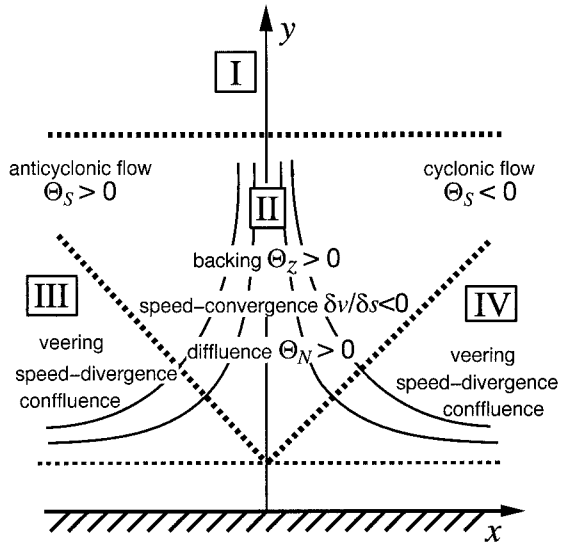

FIG. 17. Schematic showing the properties of the impinging process found in this study. We distinguish four areas (I, II, III, and IV). In area I (far upstream) the stagnation surface is not normal to the coast and is not considered as being in the impinging region proper; the impinging region is referred to in the text as formed by area II (upstream the stagnation point) and areas III and IV (past the stagnation point, symmetric).

($\Theta_Z < 0$), and therefore by positive streamwise pseudovorticity ($-v_h\Theta_Z > 0$). While in area I the magnitude of the deformation and rotation are similar ($W_K \approx 1$), in areas II, III, and IV, which correspond to the upstream and past the stagnation point regions, the magnitude of deformation exceeds the magnitude of rotation ($W_K < 1$). This fact is related to the divergence of the acceleration field. As the current approaches the coast there occurs a rotation (relative to the flow direction) of the stretching axes of the fluid element in such a way that they become almost parallel and normal to the coast in the impinging region.

The main general result of the present study is that, if it were not clear enough, there is an interaction between the current and the coast; that is, the current *really* impinges on the coast (for a rotating observer) and is deflected by the coast. Whereas, after looking at the satellite image (Fig. 2) and the density distribution (Fig. 3), our intuition tells us that this interaction is evident: the quantitative analysis of vorticity and deformation that we have done is the objective way of expressing this fact and describing how this coast–jet interaction takes place. This impinging process pattern in the Alboran Sea, while it appears to be the most frequent one, is not the only one possible. An interesting different case was observed by García-Lafuente et al. (1997), in which the AJ was ''prematurely'' deflected to the east by the presence of a small-scale cyclonic eddy located in the impinging region.

To first order the AJ impinging process is considered a quasi-steady process. That is, the temporal scale associated with the water elements passing through the impinging region (about one day) is considered to be small compared to the temporal scale of the impinging process itself. Probably the shorter periodic phenomenon that can substantially affect the impinging process is the quasiperiodic 9-day oscillation of the AJ reported by Perkins et al. (1990). Large-scale low-frequency variability in the Alboran Sea has been studied only from remote sensing data (Heburn and La Violette 1990; Vázquez-Cuervo et al. 1996). A time sequence of a part of the semiannual cycle of residual sea level in the Alboran Sea is shown in Fig. 18. The semiannual cycle was calculated by fitting at each grid point a semiannual harmonic to the merged TOPEX/Poseidon *ERS1* altimeter data from October 1992 to December 1993. This dataset was processed by fitting the TOPEX/Poseidon orbit to the *ERS1* orbit [which reduces substantially the orbit error of the *ERS1* data; see Ayoub et al. (1997) for more information on the data processing]. It was found that in the Alboran Sea the annual and semiannual cycle each account for nearly 50% of the resolved variability. Clearly visible is an eastward propagation of the semiannual wave. It therefore appears that the impinging jet process could also have relevant annual and semiannual components. However, it is important to note that the total amplitude of the temporal variability of sea level (~10 cm) is smaller than the mean sea level anomaly in the WAG–AJ system (~25 cm, e.g., Perkins et al. 1990). Thus, for example, the meridional currents at the coast near 4°W are always directed toward the coast (southward) even though the disturbance currents inferred from the sea level gradients in Fig. 18 show a reversal.

Some of the experimental results shown here for the 2D flow are in qualitative agreement with the characteristics of the flow $\mathbf{v}_\psi \equiv -\mathbf{k} \times \text{grad}_h\psi$ described by the streamfunction $\psi \equiv kxy$ (Fig. 1). The field $\mathbf{v}_\psi$ is nondivergent, and the speed divergence $\delta v_\psi/\delta s_\psi = (x^2 - y^2)/(x^2 + y^2)$ is zero when $x = y$, negative when $|x| < |y|$ and positive otherwise, which qualitatively corresponds to the speed-divergence pattern shown in Fig. 17 for areas II, III, and IV. Since $\mathbf{L}_\psi \equiv \text{grad}\ \mathbf{v}_\psi = k(\mathbf{i} \otimes \mathbf{i} - \mathbf{j} \otimes \mathbf{j})$, the directions $\mathbf{i}$ and $\mathbf{j}$ have been chosen to be the principal axes of stretching axes of the flow $\mathbf{v}_\psi$, and $\mathbf{D}_\psi = \mathbf{L}_\psi$, $\mathbf{W}_\psi = \mathbf{0}$. However, this 2D streamfunction cannot account for the 3D characteristics (z dependence) of the impinging process found in this study. Considering $\mathbf{v}_\psi$ a model of the 2D circulation, where vertical motion is not taken into account, the 3D flow is described by a set of streamfunctions ψ_i, for $i = 1, \ldots, N$, with N being the number of vertical levels. In such a flow description the property of irrotationally of every $\mathbf{v}_{\psi_i}$ may be judged by considering the relative importance of the vorticity term in the horizontal acceleration field of the impinging current. We therefore interpret that the relative rotation is negligible if the relative vorticity term of the relative acceleration field may be neglected (Truesdell 1953). This analysis is done

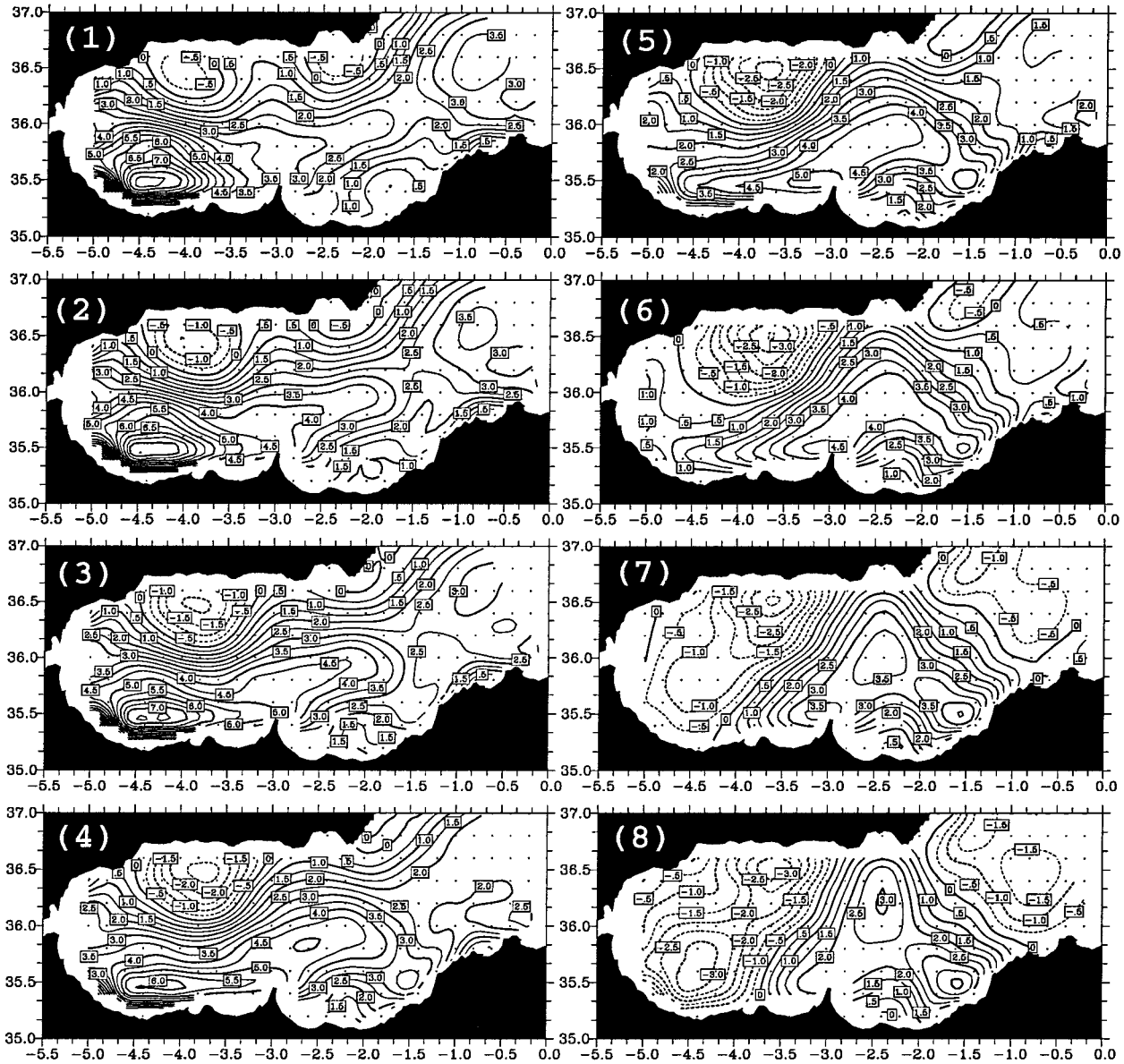

FIG. 18. Time sequence showing a part of the semiannual cycle of residual sea level in the Alboran Sea. Graphs are separated by approximately 7 days, from top to bottom and from left to right, corresponding to days 106, 113, 120, 126, 132, 139, 145, and 153 of 1993. The dots indicate the data points ($\Delta = 0.5$ cm).

by using the Lagrange formula for the 2D acceleration field

$$\mathbf{a}_h = \frac{\partial \mathbf{v}_h}{\partial t} + \zeta_3 \mathbf{k} \times \mathbf{v}_h + \frac{1}{2}\text{grad}_h v_h^2. \qquad (23)$$

A measure of the relative importance of the vorticity can therefore be obtained using the ratio

$$W_D \equiv \|\zeta_3 \mathbf{k} \times \mathbf{v}_h\| \Big/ \left\|\partial \mathbf{v}_h/\partial t + \frac{1}{2}\text{grad}_h v_h^2\right\|, \qquad (24)$$

which is a 2D version of the *dynamical vorticity number* introduced by Truesdell (1953, 1954). Note that W_D is a purely kinematic quantity and that, unlike W_K, is not Galilean invariant. The value W_D gives an indication of the importance of the rotational term in the acceleration field as written in *one particular frame.* In the steady state, W_D represents the ratio between the vertical component of the relative vorticity and the magnitude of the speed gradient ($|\zeta_3|/\|\text{grad}_h v_h\|$). The distributions of ζ_3, $\|\text{grad}_h v_h\|$ and $|\zeta_3|/\|\text{grad}_h v_h\|$ (Fig. 10c and Figs. 19a,b respectively) show that $W_D > 1$ in the water parcels of the AJ (and not in the WAG) before arriving to the impinging region. However, when the AJ and the right flow branch are deflected by the coast, the rotational

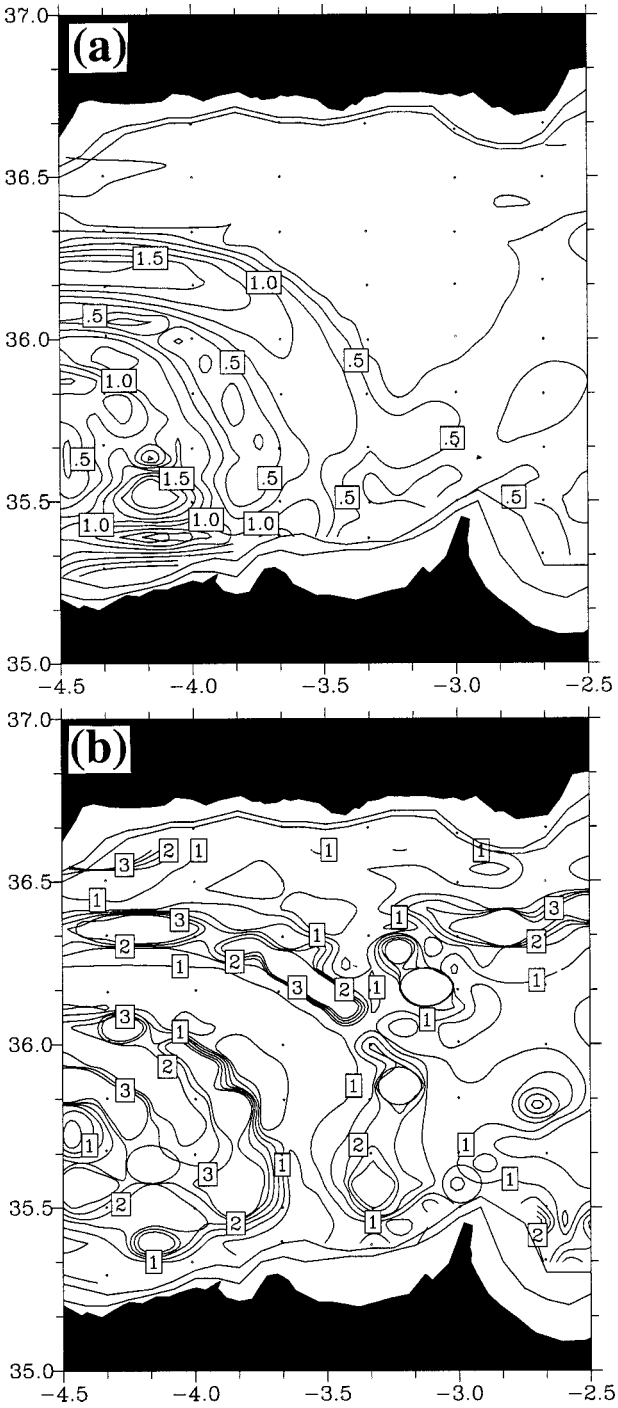

FIG. 19. Distribution at 100 m of (a) the magnitude of the horizontal speed gradient $\|\text{grad}_h v_h\|$, ($\Delta = 0.25 \times 10^{-5}$ s^{-1}); and (b) the ratio between the vertical component of the relative vorticity and the magnitude of the horizontal speed gradient $|\zeta_3|/\|\text{grad}_h v_h\|$, (contour lines from 0 to 3 by $\Delta = 0.5$).

term becomes important except in a narrow area in the impinging region where $W_D < 1$. The above results provide the spatial scale in the impinging region where the rotational term is negligible in the acceleration field, and therefore provide the spatial scale where irrotational streamfunctions like ψ may be applied.

In order to compare the impinging process in the Alboran Sea with the analytical results of Whitehead (1985b) it is required to assign an asymptotic angle of incidence to the impinging current. Because the impinging current has streamline curvature, there is no objective way for providing such an angle of incidence. Assuming that this angle is taken as zero, that is, the impinging jet is consider to be normal to the wall, Whitehead's results predict that the percent volume of fluid deflected to the right is 65% and 75% for the zero- and constant-potential-vorticity jets, respectively. The geostrophic transport function computed from the same data we have analyzed (Viúdez et al. 1996a, Fig. 13) shows that the deflected geostrophic transport is ~2 Sv (Sv $\equiv 1 \times 10^6$ m^3 s^{-1}) to the right (WAG), and ~1 Sv to the left (AJ). This corresponds to 66% of volume deflected to the right, a result that is consistent with Whitehead's theory in spite of the different jet configurations and different wall geometry (vertical vs sloping coastal boundary).

On the other hand, Whitehead and Miller (1979) and Whitehead (1985a), based on their laboratory simulation of the WAG, pointed out that the growth of the gyre may be due to the position of the stagnation point of the jet relative to coastal features. In their simulations the growing of the gyre was stopped by the basin geometry. However, since the WAG is rarely found to occupy the entire upper layer of the western Alboran basin [we know of very few cases when this happened (Lanoix 1974; Cano 1978)], it appears that, for some reason, these laboratory experiments exaggerated the effect of the impinging process on the WAG circulation. It should also be noted that in the laboratory experiments with approximate coastal geometry (Whitehead and Miller 1979) it was required to smooth Cape Tres Forcas (the cape located on the African coast at 3°W) from the coastal geometry in order to develop a gyre.

The results concerning the impinging process, based on CTD data, show that, since the stagnation surface is tilted in the vertical, the magnitude of the streamwise vorticity increases due to the vertical shear in the across stream direction with the upper layer flowing to the left (facing downstream) and the lower layer flowing to the right. The impinging process described here is therefore a 3D feature. We, however, consider that no further conclusions concerning the remote origin of the water on both sides of the stagnation surface can be made from the CTD results presented here. Two main effects prevent us from this, namely, (i) the discrete CTD sampling and (ii) the diabatic and frictional effects that prevent surfaces of constant potential density and surfaces of constant potential vorticity from being material surfaces.

We would like to emphasize that the results presented here have been concerned with the so-called *external flow* and not with the turbulent flow in the viscous region. Although we have borrowed this flow division

from the more general impinging process in fluid mechanics without proving it totally (because of the lack of measurements over the continental shelf), some results presented here (especially those concerning the irrotational characteristics of the impinging flow) point out that such a division may be acceptable in the oceanographic context. As a further consequence, since the impinging current has streamwise vorticity, it would be interesting to verify experimentally if vorticity amplification and an increase of turbulence occur over the African continental shelf, as it occurs in quasi two-dimensional impinging (nongeophysical) flows. Another possible phenomenon associated with an impinging process that may deserve further study in the oceanic case is the existence of hydraulic jumps, or standing waves, (e.g., Watson 1964; Higuera 1994; Fedorov and Melville 1996). If such a hydraulic jump exists, it could be observed along the African coast.

Impinging jet processes have received little attention in physical oceanography. For example, the study about the opposite phenomenon, that is, coastal current separation, is much more developed (e.g., Ou and De Ruijter 1986; Page 1987; Signell and Geyer 1991; Klinger 1994). We think that this is because the impingment process, although it may occur frequently in the ocean, is not usually a steady process (the temporal evolution of an eddy forced against a boundary has been studied by Shi and Nof 1993). Our main objective has been therefore to study, in a broad way, the main kinematic characteristics of an impinging jet in the Alboran Sea, and to relate this process with other disciplines of fluid mechanics. Since the presence the Atlantic jet is assured by the location of the Strait of Gibraltar, the impingment process in the Alboran Sea case is, concerning the steadiness, a *privileged* one.

4. Summary

We have described an oceanic impinging jet process in terms of its density, curvatures, backing, vorticity, and deformation characteristics. In the impingment region the acceleration field is divergent, which is related to the fact that the magnitude of deformation is larger than the magnitude of rotation. It also has been found that the stagnant streamsurface does not lie in a vertical plane but tilts in the opposite direction to the vertical tilting of isopycnals. The flow upstream of the stagnation point is characterized by backing, speed convergence, diffluence, and negative streamwise vorticity. The flow past the stagnation point is characterized by veering, speed divergence, confluence, and positive streamwise vorticity. The stretching axes of a fluid element approaching the coast experience a rotation relative to the flow direction in such a way that they become almost parallel and normal to the coast in the impinging region. Only in a narrow area of that impinging region can the current be considered irrotational.

Acknowledgments. The authors greatly appreciate a postdoctoral grant from the Ministerio Español de Educación y Ciencia and support from the Office of Naval Research (Code 322). N. Ayoub and P. Y. Le Traon are thanked for providing the altimetric dataset. One of the authors (J.V.-C.) is under contract with the National Aeronautics and Space Administration.

APPENDIX

The Stretching Tensor of the Horizontal Flow

In order to consider the different scales of the horizontal and vertical components of the velocity we again make use of (21) and write

$$\mathbf{D} = \frac{1}{2}(\mathbf{L}_h + \mathbf{L}_h^{\mathrm{T}}) + \frac{1}{2}(\mathbf{v}_{h,3} \otimes \mathbf{k} + \mathbf{k} \otimes \mathbf{v}_{h,3}) + \frac{1}{2}(\mathbf{k} \otimes \mathrm{grad}\upsilon_3 + \mathrm{grad}\upsilon_3 \otimes \mathbf{k}) \equiv \mathbf{D}_h + \mathbf{D}_Z + \mathbf{D}_W, \quad \text{(A1)}$$

where $\mathbf{D}_h$, $\mathbf{D}_Z$, and $\mathbf{D}_W$ are the symmetric tensors associated to the horizontal deformation, vertical shearing, and deformation induced by the gradient of the vertical velocity, respectively. If $\mathbf{v}_{h,3} = \upsilon_{\alpha,3}\mathbf{e}_\alpha$ in the $\{\mathbf{e}_i\}$ frame, we have $\mathbf{D}_Z = (\frac{1}{2})\upsilon_{\alpha,3}(\mathbf{e}_\alpha \otimes \mathbf{k} + \mathbf{k} \otimes \mathbf{e}_\alpha)$. Since the magnitude of the components $\upsilon_{\alpha,3}$ in the impinging current is two orders of magnitude larger than the magnitude of the largest components of $\mathbf{D}_h$, and since $\upsilon_3/\upsilon_h = O(10^{-3})$, the dominant term on the right-hand side

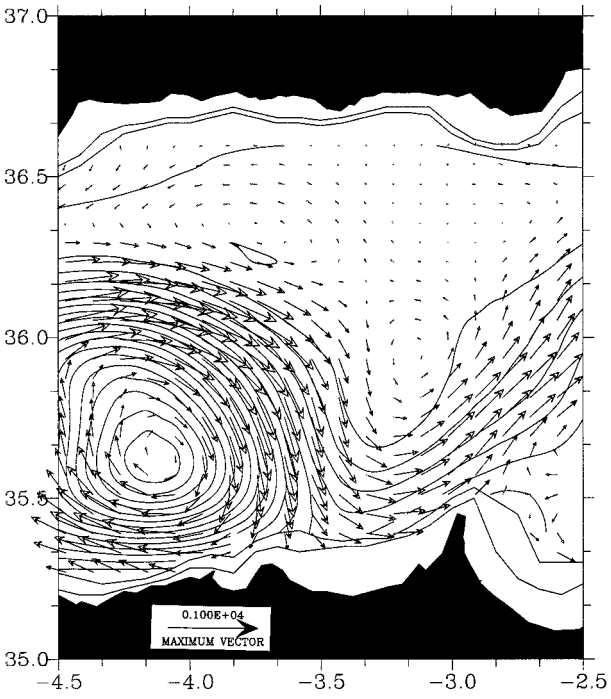

FIG. A1. Distribution of $\mathbf{v}_{h,3}$ at 100 m. Reference vector is 10^{-2} s^{-1}. Thin isolines represent pressure anomalies.

of (A1) is $\mathbf{D}_Z$. Introducing the field of unit director vectors $\mathbf{e}_Z(\mathbf{x}) \equiv \mathbf{v}_{h,3}/\|\mathbf{v}_{h,3}\|$ of the vertical shear $\mathbf{v}_{h,3}$ (for $\|\mathbf{v}_{h,3}\| \neq 0$) we write $\mathbf{v}_{h,3} = \|\mathbf{v}_{h,3}\|\mathbf{e}_Z$ and $\mathbf{D}_Z = (\frac{1}{2})\|\mathbf{v}_{h,3}\|(\mathbf{e}_Z \otimes \mathbf{k} + \mathbf{k} \otimes \mathbf{e}_Z)$. Thus, the two nonzero proper values of $\mathbf{D}_Z$ are $\pm (\frac{1}{2})\|\mathbf{v}_{h,3}\|$ and the corresponding field of proper vectors are $2^{-1/2}(\mathbf{e}_Z \pm \mathbf{k})$. Therefore, the stretching axes of the 3D flow lay approximately in the vertical plane parallel at every point to $\mathbf{v}_{h,3}$, and forming 45° angle with the horizontal plane. Furthermore, since $\mathbf{v}_{h,3} = (\upsilon_h \mathbf{s}_h)_{,3} = \upsilon_{h,3}\, \mathbf{s}_h + \upsilon_h \Theta_Z \mathbf{n}_h$, and $\upsilon_{h,3} \gg \upsilon_h \Theta_Z$, the direction of $\mathbf{v}_{h,3}$ is very close to the direction $\mathbf{s}_h$ (Fig. A1), and the stretching axes of the 3D flow lay very approximately in vertical planes tangent at every point to the horizontal velocity vector. Since the stretching tensor $\mathbf{D}$ is dominated by the large values of $\mathbf{v}_{h,3}$, a direct representation of the stretching axes of the 3D flow is, in general, unsuitable.

REFERENCES

Ayoub, N., P. Y. Le Traon, and P. De Mey, 1997: A description of the Mediterranean surface variable circulation from combined ERS-1 and TOPEX/POSEIDON altimetric data. *J. Mar. Syst.*, in press.

Batchelor, G. K., 1970: *An Introduction to Fluid Dynamics*. Cambridge University Press, 615 pp.

Bjørgum, O., 1951: On Beltrami vector fields and flows. Part I. Universitet J. Bergen, Naturvitenskapalig rekke, No. 1, 1–85.

Brandes, E. A., R. P. Davies-Jones, and B. C. Johnson, 1988: Streamwise vorticity effects on supercell morphology and persistence. *J. Atmos. Sci.*, **45,** 947–963.

Bucca, P. J., and T. H. Kinder, 1984: An example of meteorological effects on the Alboran Sea gyre. *J. Geophys. Res.*, **89,** 751–757.

Cano, N., 1978: Hidrología del Mar de Alborán en primavera-verano. *Bol. Inst. Esp. Oceanogr.,* **248,** 51–66.

Chadwick, P., 1976: *Continuum Mechanics*. Wiley, 174 pp.

Churchill, S. W., 1988: *Viscous Flows: The Practical Use of Theory*. Butterworth, 602 pp.

Conlon, D. M., 1982: On the outflow mode of the Tsugaru Warm Current. *La Mer,* **10,** 60–64.

Davies-Jones, R., 1984: Streamwise vorticity: The origin of updraft rotation in supercell storms. *J. Atmos. Sci.,* **41,** 2991–3006.

——, 1991: The frontogenetical forcing of secondary circulations. Part I: The duality and generalization of the Q vector. *J. Atmos. Sci.,* **48,** 497–509.

Dhanak, M. R., and J. T. Stuart, 1995: Distorsion of the stagnation-point flow due to cross-stream vorticity in the external flow. *Philos. Trans. Roy. Soc. London,* A, **352,** 443–452.

Dorrepaal, J. M., 1986: An exact solution of the Navier-Stokes equation which describes non-orthogonal stagnation-point flow in two dimensions. *J. Fluid Mech.,* **163,** 141–147.

Ericksen, J. L., 1960: Tensor fields. *Handbuch der Physik* III/I, S. Flügge, Ed., Springer-Verlag, 794–858.

Fedorov, A. V., and W. K. Melville, 1996: Hydraulic jumps at boundaries in rotating fluids. *J. Fluid Mech.,* **324,** 55–82.

Ferri, A., and P. A. Libby, 1954: Note on an interaction between the boundary layer and the inviscid flow. *J. Aeronaut. Sci.,* **21,** 130.

García-Lafuente, J., N. Cano, M. Vargas, J. P. Rubín, and A. Hernández-Guerra, 1997: Evolution of the Alboran Sea hydrographic structures during July 1993. *Deep-Sea Res.,* in press.

Gascard, J. C., and C. Richez, 1985: Water masses and circulation in the western Alboran Sea and in the Straits of Gibraltar. *Progress in Oceanography,* Vol. 15, Pergamon Press, 157–216.

Gluert, M. B., 1957: The boundary layer in simple shear flow past a flat plate. *J. Aeronaut. Sci.,* **24,** 848–849.

Godske, C. L., T. Bergeron, J. Bjerknes, and R. C. Bundgaard, 1957: *Dynamic Meteorology and Weather Forecasting.* Amer. Meteor. Soc. and Carnegie Institute, 800 pp.

Goląb, S., 1974: *Tensor Calculus.* Elsevier, 371 pp.

Gurtin, M., 1981: *An Introduction to Continuum Mechanics.* Academic Press, 265 pp.

Haney, R. L., 1974: A numerical study of the response of an idealized ocean to large-scale surface heat and momentum flux. *J. Phys. Oceanogr.,* **4,** 145–167.

——, 1985: Midlatitude sea surface temperature anomalies: A numerical hindcast. *J. Phys. Oceanogr.,* **15,** 787–799.

Hawthorne, W. R., 1951: Secondary circulation in fluid flow. *Proc. Roy. Soc. London Ser.* A, **206,** 374–387.

——, and M. E. Martin, 1955: The effect of density gradient and shear on the flow over a hemisphere. *Proc. Roy. Soc. London Ser.* A, **232,** 184–195.

Heburn, G. W., and P. E. La Violette, 1990: Variations in the structure of the anticyclonic gyres found in the Alboran Sea. *J. Geophys. Res.,* **95,** 1599–1613.

Hiemenz, K., 1911: Die Grenzschicht an einem in den gleichförmigen Flüssigkeitsstrom eingetauchten geraden Kreiszylinder. Ph.D. dissertation, Göttingen and Dingl. Polytech. J.

Higuera, F. J., 1994: The hydraulic jump in a viscous laminar flow. *J. Fluid Mech.,* **274,** 69–92.

Hollmann, G., 1958: Die Krümmungs- und die Scherungs-Vorticitygleichung; Die Richtungs- und die Geschwindigkeits-Divergenzgleichung. *Beitr. Phys. Atmos.,* **30,** 254–267.

Hoskins, B. J., 1975: The geostrophic momentum approximation and the semi-geostrophic equations. *J. Atmos. Sci.,* **32,** 233–242.

Howarth, L., 1935: On the calculation of steady flow in the boundary layer near the surface of a cylinder in a stream. *Aero. Res. Counc., Lond., R&M* no. 1632.

Kawasaki, Y., and T. Sugimoto, 1984: Experimental studies on the formation and generation processes of the Tsugaru Warm Gyre. *Ocean Hydrodynamics of the Japan and East China Seas*, T. Ichiye, Ed., Oceanogr. Series, No. 39, Elsevier, 225–238.

Kemp, N. H., 1959: Vorticity interaction at an axisymmetric stagnation point in a viscous incompressible fluid. *J. Aerosp. Sci.,* **26,** 543–544.

Klinger, B. A., 1994: Inviscid current separation from rounded capes. *J. Phys. Oceanogr.,* **24,** 1805–1811.

La Violette, P. E., 1986: Short term measurements of surface currents associated with the Alboran Sea during ¿Donde Va? *J. Phys. Oceanogr.,* **16,** 262–279.

Lakshminarayana, B., and J. H. Horlock, 1973: Generalized equations for secondary vorticity using intrinsic co-ordinates. *J. Fluid Mech.,* **59,** 97–115; Corrigendum, **226,** 661–663.

Lanoix, F., 1974: Projet Alboran, Etude hydrologique et dynamique de la Mer d'Alboran. Tech. Rep. 66, NATO, Brussels, 39 pp. plus 32 figs. [Available from NATO Subcommittee on Oceanographic Research, Copenhagen, Denmark.]

Li, T. Y., 1955: Simple shear flow past a flat plate in an incompressible fluid of small viscosity. *J. Aeronaut. Sci.,* **22,** 651–652.

——, 1956: Effects of free-stream vorticity on the behaviour of a viscous boundary layer. *J. Aeronaut. Sci.,* **23,** 1128–1129.

Lynch, P., and X.-Y. Huang, 1992: Initialization of the HIRLAM model using a digital filter. *Mon. Wea. Rev.,* **120,** 1019–1034.

Marris, A. W., 1964: Generation of secondary vorticity in a stratified fluid. *J. Fluid Mech.,* **20,** 117–181.

——, and S. L. Passman, 1968: Vector fields and flows on developable surfaces. *Arch. Ration. Mech. Anal.,* **31,** 29–86.

Masotti, A., 1927: Decomposizione intrinseca del vortice e sue applicazioni. *Inst. Lombardo Sci. Lett. Rendiconti,* **60**(2), 869–874.

Morse, P. M., and H. Feshbach, 1953: *Methods of Theoretical Physics. Part I.* McGraw-Hill, 997 pp.

Onken, R., 1990: The creation of reversed baroclinicity and subsurface jets in oceanic eddies. *J. Phys. Oceanogr.,* **20,** 786–791.

Ou, H. W., and W. P. M. De Ruijter, 1986: Separation of an inertial boundary current from a curved coastline. *J. Phys. Oceanogr.,* **16,** 280–289.

Page, M. A., 1987: Separation and free-streamlines flows in a rotating fluid at low Rossby number. *J. Fluid Mech.,* **179,** 155–177.
Parrilla, G., and T. H. Kinder, 1987: The physical oceanography of the Alboran Sea. *Rep. Meteor. Oceanogr.,* **1,** 143–184.
——, ——, and R. H. Preller, 1986: Deep and intermediate Mediterranean water in the western Alboran Sea. *Deep-Sea Res.,* **33,** 55–88.
Pedlosky, J., 1987: *Geophysical Fluid Dynamics.* 2d ed. Springer-Verlag, 710 pp.
Peregrine, D. H., 1981: The fascination of fluid mechanics. *J. Fluid Mech.,* **106,** 59–80.
Perkins, H., T. Kinder, and P. E. La Violette, 1990: The Atlantic inflow in the western Alboran Sea. *J. Phys. Oceanogr.,* **20,** 242–263.
Rott, N., and M. Lenard, 1959: Vorticity effect on the stagnation-point flow of a viscous incompressible fluid. *J. Aerosp. Sci.,* **26,** 542–543.
Sadeh, W. Z., and H. J. Brauer, 1980: A visual investigation of turbulence in stagnation flow about a circular cylinder. *J. Fluid Mech.,* **99,** 53–64.
Schlichting, H., 1979: *Boundary-Layer Theory.* McGraw-Hill, 817 pp.
Schouten, J. A., 1954: *Ricci-Calculus. An Introduction to Tensor Analysis and Its Geometrical Applications.* 2d ed. Springer-Verlag, 516 pp.
Scorer, R. S., 1978: *Environmental Aerodynamics.* Ellis Horwood, 488 pp.
——, and S. D. R. Wilson, 1963: Secondary instability in steady gravity waves. *Quart. J. Roy. Meteor. Soc.,* **89,** 532–539.
Shi, C., and D. Nof, 1993: The splitting of eddies along boundaries. *J. Mar. Res.,* **51,** 771–795.
Signell, R. P., and W. R. Geyer, 1991: Transient eddy formation around headlands. *J. Geophys. Res.,* **96,** 2561–2575.
Speziale, C. G., 1987: On helicity fluctuations in turbulence. *Quart. Appl. Math.,* **45,** 123–129.
Squire, H. B., and G. Winter, 1951: The secondary flow in a cascade of airfoils in a nonuniform stream. *J. Aeronaut. Sci.,* **18,** 271–277.
Stuart, J. T., 1959: The viscous flow near a stagnation point when the external flow has uniform vorticity. *J. Aerosp. Sci.,* **26,** 124–125.
Sutera, S. P., 1965: Vorticity amplification in stagnation-point flow and its effect on heat transfer. *J. Fluid Mech.,* **21,** 513–534.
——, P. F. Maeder, and J. Kestin, 1963: On the sensitivity of heat transfer in the stagnation-point boundary layer to free-stream vorticity. *J. Fluid Mech.,* **16,** 497–520; Corregendum, **17,** 480.
Tai, C.-T., 1992: *Generalized Vector and Dyadic Analysis.* IEEE Press, 134 pp.
Truesdell, C., 1953: Two measures of vorticity. *J. Ration. Mech. Anal.,* **2,** 173–217.
——, 1954: *Kinematics of Vorticity.* Indiana University Press, 232 pp.
——, 1991: *A First Course in Rational Continuum Mechanics.* Vol. 1. 2d ed. Academic Press, 391 pp.
——, and R. Toupin, 1960: The classical field theories. *Handbuch der Physik III/I,* S. Flügge, Ed., Springer-Verlag, 902 pp.
Vázquez-Cuervo, J., J. Font, and J. J. Martínez-Benjamín, 1996: Observations on the circulation in the Alboran Sea using *ERS1* altimetry and sea surface temperature data. *J. Phys. Oceanogr.,* **26,** 1426–1447.
Viúdez, A., and R. L. Haney, 1996: On the shear and curvature vorticity equations. *J. Atmos. Sci.,* **53,** 3384–3394.
——, J. Tintoré, and R. L. Haney, 1996a: Circulation in the Alboran Sea as determined by quasi-synoptic hydrographic observations. Part I: Three-dimensional structure of the two anticyclonic gyres. *J. Phys. Oceanogr.,* **26,** 684–705.
——, R. L. Haney, and J. Tintoré, 1996b: Circulation in the Alboran Sea as determined by quasi-synoptic hydrographic observations. Part II: Mesoscale ageostrophic motion diagnosed through density dynamical assimilation. *J. Phys. Oceanogr.,* **26,** 706–724.
Watson, E. J., 1964: The radial spread of a liquid jet over a horizontal plane. *J. Fluid Mech.,* **20,** 481–499.
Whitehead, J. A., Jr., 1985a: A laboratory study of gyres and uplift near the Strait of Gibraltar. *J. Geophys. Res.,* **90,** 7045–7060.
——, 1985b: The deflection of a baroclinic jet by a wall in a rotating fluid. *J. Fluid Mech.,* **157,** 79–93.
——, and A. R. Miller, 1979: Laboratory simulations of the gyre in the Alboran Sea. *J. Geophys. Res.,* **84,** 3733–3742.